# SILICON SOLAR CELLS: CHARACTERIZATION AND MODELLING

By

DOMINIC J. MBEWE

A THESIS

PRESENTED TO THE UNIVERSITY OF MANITOBA

IN PARTIAL FULFILMENT OF THE

REQUIREMENTS FOR THE DEGREE

OF MASTER OF SCIENCE

IN

ELECTRICAL ENGINEERING

WINNIPEG, MANITOBA

1982

# SILICON SOLAR CELLS: CHARACTERIZATION AND MODELLING

BY

DOMINIC J. MBEWE

A thesis submitted to the Faculty of Graduate Studies of
the University of Manitoba in partial fulfillment of the requirements
of the degree of

MASTER OF SCIENCE

I authorize the University of Manitoba to lend this thesis to other institutions or individuals for the purpose of scholarly research.

Dominic J. Mbewe

I further authorize the University of Manitoba to reproduce this thesis or by other means, in total or in part at the request of other institutions or individuals for the purpose of scholarly research.

Dominic J. Mbewe

CONTENTS

ABSTRACT

This thesis is in two parts (a) and (b). Part (a) involves an experimental characterization of the spectral properties of silicon solar cells. Part (b) is concerned with the theoretical modelling of silicon solar cells for operation under concentrated sunlight conditions.

(a) Experimental observations are presented concerning the dependence of the spectral response of silicon photovoltaic cells upon the optical illumination intensity. These effects are significant only in silicon materials with many extended defects: grain boundaries and dislocations. In this case, the short-circuit current response to a chopped monochromatic optical excitation increases monotonically as a background optical (white light) bias is increased to approximately AM1 intensity. These results may be explained in terms of SRH recombination through defect states at grain boundaries and dislocations which under these conditions enter a high-injection regime at the defect sites, as a result of their associated space-charge regions. This mechanism helps to explain the observation that the photocurrents in solar cells made from cast polycrystalline silicon are not appreciably lower than for crystalline silicon.

(b) The design of photovoltaic (PV) and photovoltaic/thermal (PV/T) solar energy conversion systems employing optical concentration requires simple models of solar cells which nevertheless have sufficient accuracy to be employed in design decisions. Semiempirical expressions are presented for open-circuit voltage, short-circult current, fill factor, and conversion efficiency of silicon solar cells as explicit functions of optical concen-

tration (C) and temperature (T). In addition similar expressions are given for the solar cell current as a function of C and T and of the operating voltage V, to enable characterization under conditions of non-optimal power transfer. The agreement of the model with experimental data is shown to be within ≅ 10% for all parameters. An example of an application of the model to system design is also presented.

## ACKNOWLEDGMENTS

I wish to thank Professor H. C. Card for his supervision, direction and guidance in this research. Thanks also go to Professor D. C. Card of the Mechanical Engineering Department of the University of Manitoba for his contributions related to the design example of solar concentrator photovoltaic/thermal system. D. J. Thomson and R. D. McLeod have contributed substantially to the experimental work on the spectral response of cast silicon solar cells. Chapter 2 therefore represents a joint effort with these students. I am very grateful for their participation in this project. Discussions with Professor K. C. Kao, Y. P. Hsieh, A. W. DeGroot, G. C. McGonigal and J. G. Shaw of Materials and Devices Laboratory of the Electrical Engineering Department of the University of Manitoba are much appreciated. The author also acknowledges the financial support of the Natural Sciences and Engineering Research Council of Canada (NSERC) under strategic Grant G0442.

# CHAPTER 1

## 1.1 Introduction

This thesis consists of two separate investigations of silicon solar cells. The first part, (a) deals with intensity dependence of the spectral response of cast (large-grained) polycrystalline silicon solar cells and its interpretation in terms of high-level injection conditions at extended defects which are useful in the design of concentrator photovoltaic/thermal systems.

(a) There have recently been a number of experimental reports of an increase in the minority carrier diffusion length, L, or lifetime, $\tau$ , with optical illumination intensity in silicon solar cells.[1-8] It is generally observed that L increases substantially, even at low intensities (below AM1), for material such as EFG ribbon silicon,[3-5] whereas in crystalline (Czochralski or float-zone) silicon these effects are observed only under strongly concentrated sunlight intensities.[2, 6-8] The explanations for these observations have involved isolated trapping centers, and have invoked the suggestions of trap saturation[1] and/or traps with multiple energy levels.[2-5]

In this thesis, we present new data concerning the dependence of quantum efficiency vs. wavelength upon the intensity of optical (white-light) bias, for silicon photovoltaic cells made from both cast (large-grained) polycrystalline silicon and crystalline silicon. We also show that the observed behavior is consistent with minority carrier recombinations at either grain boundaries or dislocations. As a result of the

space-charge regions adjacent to these extended defects, [9-11] conditions of high-level injection can occur in the polycrystalline material at relatively low optical intensities. It is the high-level injection condition, we argue, that causes the increase in carrier lifetime in accordance with Shockley-Read-Hall (SRH) statistics.[12, 13] Neither trap saturation nor multi-level centers are required for this mechanism, although these complications may certainly be present in some cases. In crystalline material, recombination occurs primarily through isolated point defect centers, and in this case, high-level injection is reached only under extremely high optical intensities for typical base doping levels of silicon solar cells.[14] Such intensities are only obtained in strongly concentrated sunlight (typically 100-1000 suns).

(b) One of the more promising approaches to reducing the cost of photovoltaic solar energy conversion is the use of optical concentrators such as Fresnel lenses. Only a small fraction of the optical collection area (as little as one percent for silicon cells) is then required to be covered by the solar cells which are the expensive component of the system.[22-26] The conversion efficiency also improves with concentration.

For relatively large concentration ratios, active cooling is normally required to minimize the temperature of the solar cells, since the photovoltaic efficiency is degraded by elevated temperatures.[23] At a concentration ratio of 100, for example, the total optical power incident upon the solar cell is approximately 10 W $cm^{-2}$. Active cooling can, in some applications, also be used to provide useful thermal energy.

In the design of the overall energy conversion system, and in particular in the design of the cooling apparatus, it is important to have a relatively simple model of the solar cells which nevertheless gives a sufficiently accurate prediction of the dependence of the photovoltaic parameters on both the optical intensity and temperature. There have been previous studies on the physics of solar cells under concentrated sunlight [22-40], primarily under laboratory conditions in which the cells were maintained at room temperature. Additional investigations of the effects of temperature have been reported[23, 27, 31, 40-42], generally under unconcentrated solar illumination.

This thesis develops a model of solar cells which we feel can be useful in concentrator photovoltaic/thermal system design. The representation takes account of all aspects of device physics which have important effects upon the photovoltaic parameters, but at the same time is sufficiently simple to be of benefit to system designers who may be unfamilar with the details of this physics. Both the optical concentration (C) and the operating temperature (T) appear explicitly in the expressions for the photovoltaic parameters.

# CHAPTER II

# High-Injection Conditions at Extended Defects in Silicon: A Mechanism for Dependence of Lifetime on Photogeneration Rate

## 2.1 Experimental

The cast polycrystalline silicon used in the present studies was p-type 'Silso' material with an acceptor concentration $N_a = 3 \times 10^{15}$ cm$^{-3}$ obtained from Wacker Chemitronic, Inc. Solar cell structures were of the 'minMIS' minority-carrier grating type, described by Green[15] and others. Details on the fabrication, performance, and geometry of our devices are described elsewhere;[16] it is sufficient to mention here that the active area was 0.8 cm$^2$ and the open-circuit voltage, short circuit current density and active-area efficiency were 0.48 V, 30 mA cm$^{-2}$, and 10.3% respectively under AM1 illumination conditions for the polycrystalline Si devices.

The measurements of quantum efficiency vs. wavelength were performed using the arrangement shown in Fig. 1. A monochromatic optical excitation of 50-200 μW cm$^{-2}$ was chopped at a frequency of 10 Hz, and the response (short-circuit current) was measured using phase-sensitive detection. At the same time, the sample was illuminated with an optical bias of (unchopped) white light from a General Electric ELH quartz-halogen lamp, the intensity of which was controlled using neutral density filters. Figure 2 shows a typical example of the spectral response of the polycrystalline silicon device in the absence of an optical white-light bias. Figure 3 shows the response of the same device with the intensity of the optical bias as a parameter. These results (Fig. 3) have been normalized to the response with no optical bias. It is apparent (a) that the response at longer

wavelengths increases monotonically with the intensity of the optical bias, up to a factor of approximately two. The experiment has also been performed with crystalline silicon solar cells, and up to the maximum intensity (AM1) studied here no significant enhancement of the response due to the optical bias has been observed (the response is increased by at most 1-2% by the optical bias).

## 2.2 Discussion

Our interpretation of these results as well as those concerning the dependence of minority carrier diffusion length or lifetime observed earlier[3-5] relies upon the presence of extended defects: dislocations or grain boundaries in the Wacker (and ribbon) silicon materials. It is well known that in the cast silicon material such as the Wacker Silso type used here, recombination occurs both at the grain boundaries and at dislocations within the grains themselves. Since the grain size is large, the majority of the recombination is likely to occur at dislocations. The density of these dislocations is much greater than in Czochralski or float-zone crystalline silicon material, as a result of the casting process.

Figure 4 shows the energy-band diagram in the neighborhood of a dislocation or grain boundary, as discussed previously.[10] The position (x) from the defect is measured radially in the case of a dislocation (line defect) or perpendicular from the grain boundary (planar defect).

We assume that there exists a single level of localized states or traps at the defect, which is somewhat broadened by the variation in the atomic configurations surrounding this defect. This level is approximately at midgap,

with a spread of less than 0.1 eV, as determined experimentally for silicon bicrystals or grain boundaries.[11] The origin of the primary defect is probably an unsatisfied or 'dangling' bond on a silicon atom. The density of these defects is on the order of $10^{11}$-$10^{12}$ $cm^{-2}$. [17, 18] For any appreciable illumination intensity, the quasi-Fermi levels for elctrons and holes enclose these defect centers in energy, so that all of the states in this peak contribute equally to recombination.[10, 19] According to SRH statistics the recombination rate of electrons and holes through these centers is given by [12, 10]

$$R = \frac{N_t V_{th} \sigma_n \sigma_p (pn - n_i^2)}{\sigma_n (n+n_1) + \sigma_p (p+p_1)} \qquad (1)$$

where $n$ and $p$ are the concentrations of electrons and holes at the defect site, $N_t$ is the density of traps, $V_{th}$ is the thermal velocity, $\sigma_n$ and $\sigma_p$ are the capture cross sections of the traps for electrons and holes, $n_i$ is the intrinsic carrier concentration, and

$$n_1 = n_i \exp\left(\frac{E_t - E_i}{kT}\right) \qquad (2)$$

$$P_1 = n_i \exp\left(\frac{E_i - E_t}{kT}\right) \qquad (3)$$

with $E_i$ the intrinsic (midgap) energy level and $E_t$ the energy level of the traps. To a first approximation, since we assume as discussed above that $E_t = E_i$, $n_1$ and $p_1$ are of the order of $n_i$, the intrinsic concentration.

To be specific, let us consider p-type silicon material, as in Fig. 4

and as in the samples of Figs. 2 and 3. As is known from work on silicon grain boundries, the trapping states in p-type material take on a positive charge which is compensated by a negative charge in the surrounding silicon so that a space-charge (depletion) region of uncompensated acceptors develops adjacent to the defect.[18] Parenthetically, it is significant that in n-type material the traps assume a negative charge and again a depletion region is established, this time of uncompensated donors.[17] These observations imply a neutral level for the traps near midgap, which suggests an admixture of donor-like and acceptor-like character for these traps.

The density of traps $N_t$ will determine the energy position of the equilibrium Fermi level $E_{fo}$ at the defect site, with $E_{fo}$ approaching midgap at large $N_t$. Assuming an intermediate value of $N_t$ for generality we have that $n << p$ at the defect under equilibrium (dark) conditions. Eqn. (1) therefore simplifies, near equilibrium, to

$$R = N_t V_{th} \sigma_n (n - n_o) \qquad (4)$$

where $n_1$, $p_1$ have been neglected in comparison with $p$ and $n_o$ is the equilibrium concentration of electrons at the defect.

$R$ in Eqns. (1) and (4) has units of $m^{-2}s^{-1}$ for planar defects (grain boundaries) and $m^{-1}s^{-1}$ for linear defects (dislocations). $N_t$ has units $m^{-2}$ and $m^{-1}$ in the two cases. The units of $V_{th}$, $\sigma_n$ and $n$ are $ms^{-1}$, $m^2$ and $m^{-3}$ in both cases.

In order to obtain the <u>volume</u> recombination rates, we recognize that the density of traps per unit volume is given by

$$N_{tv} = \frac{1}{V} \int_A N_t \cdot dA \qquad \text{planar defects} \qquad (5a)$$

$$= \frac{1}{V} \int_\ell N_t \cdot d\ell \qquad \text{linear defects} \qquad (5b)$$

where the integrals are over the total area or length of the defects in the sample volume. Similarly, we can write for the volume recombination rates,

$$R_v = \frac{1}{V} \int_A R \cdot dA \qquad \text{planar defects} \qquad (6a)$$

$$= \frac{1}{V} \int_\ell R \cdot d\ell \qquad \text{linear defects} \qquad (6b)$$

We can alternately write an expression for the volume recombination rates which involves the minority carrier lifetime $\tau_n$ as

$$R_v = \frac{n_v - n_{vo}}{\tau_n} \qquad (7)$$

provided $n_v << p_v$, where $n_v$ and $p_v$ are the volume concentrations of electrons and holes under conditions of optical illumination and $n_{vo}$, $p_{vo}$ are the equilibrium values of $n_i^2/N_a$ and $N_a$ respectively. $N_a$ is the acceptor doping concentration of the material.

The concentration $n_v$ of electrons in the bulk material, away from the devects, is substantially lower than $n$ at the defect site, as a consequence of the reduced potential energy for electrons there (Fig. 4).

The relation for the equilibrium (dark) case is simply

$$n_o = n_{vo} \exp(V_{do}/V_T) \tag{8}$$

where $V_{do}$ is the equilibrium diffusion potential in Fig. 4 and $V_T = kT/q$. Under conditions of optical illumination, however, the relationship of $n$ to $n_v$ is complicated by the uncertainty in the shape of the electron quasi-Fermi level $E_{fn}$ which is no longer flat through the space-charge region[19] particularly at high recombination rates. If we employ the reasonable assumption that $E_{fn}$ remains approximately flat under conditions of low illumination, and the diffusion potential is not modified from $V_{do}$, then $n$ and $n_v$ are also related by Eqn. (8).

$$n = n_v \exp(V_{do}/V_T) \tag{9}$$

for low illumination levels. Note that $V_{do}$ remains in (9) because for low photogeneration rates the diffusion potential $V_d$ maintains its equilibrium value $V_{do}$ [10,18].

Assuming defects with uniform properties over the length or area of the dislocation or grain boundary, we obtain from Eqns. (5) and (6) that

$$R_v = R \left( \frac{N_{tv}}{N_L} \right) \tag{10}$$

which with Eqns. (4), (8), and (9) gives that

$$R_v = N_{tv} V_{th} \sigma_n (n_v - n_{vo}) \exp(\frac{V_{do}}{V_T}) \tag{11}$$

Using (7),

$$\tau_n = [N_{tv} V_{th} \sigma_n \exp(V_{do}/V_T)]^{-1} \tag{12}$$

for sufficiently low photogeneration rates that the diffusion potential $V_d$ remains at its equilibrium value $V_{do}$. One can regard Eqn. (12) as the normal expression for lifetime under low-injection conditions, except that an effective capture cross section

$$\sigma_n^* = \sigma_n \exp( \frac{V_{do}}{V_T}) \tag{13}$$

is associated with the recombination centers for the extended defects.

As the photogeneration rate increases, the concentration of minority carriers at the defect $n$ increases as this is an imperfect sink for these carriers, until at a critical illumination intensity $n\,\sigma_n \cong p\,\sigma_p$ at the defect. At this point, $V_d$ will begin to decrease rapidly from its equilibrium value $V_{do}$ with further increases in illumination intensity.[10,19] This marks the onset of high injection conditions at the defect, with $n$ and $p$ increasing with illumination in such a way that $n\,\sigma_n \cong p\,\sigma_p$ thereafter.[10] Under these conditions, (1) may be rewritten as

$$R \cong \frac{N_t\, V_{th}\, \sigma_n\, n}{2} = \frac{N_t\, V_{th}\, \sigma_p\, p}{2} \tag{14}$$

and

$$R_v \cong \frac{N_{tv}\, V_{th}\, \sigma_n \exp\left(\frac{V_d}{V_T}\right) n_v}{2} \tag{15}$$

so that

$$\tau_n = 2\left[N_{tv}\, V_{th}\, \sigma_n \exp\left(\frac{V_d}{V_T}\right)\right]^{-1} \tag{16}$$

for high-level injection conditions at the defect. Thus the effective capture cross section becomes

$$\sigma_n^* = \frac{1}{2}\,\sigma_n \exp\left(\frac{V_d}{V_T}\right) \tag{17}$$

for high photogeneration rates. Eqn. (16) shows that the lifetime for high optical illumination intensities is larger than that at low intensities by at least a factor of two, and can be considerably larger for

appreciable decreases in $V_d$ below $V_{do}$.

The experimental results of Fig. 3 imply that the minority carrier diffusion length $L_n$ of the solar cell increases by a factor of approximately two as the optical intensity increases to the AM1 level, for the Wacker silicon in which the recombination is controlled by extended defects such as dislocations or grain boundaries. An observed increase in $L_n$ by a factor of two translates into an increase in minority carrier lifetime $\tau_n$ by a factor of four, since $L_n = (D_n \tau_n)^{1/2}$, which is a very reasonable value in the light of Eqn. (16). This corresponds to the observed spectral response at long wavelengths (near-uniform photogeneration) which increases by this same factor of two.

It is important to note that the optical intensity required for the onset of the increased lifetime may be relatively low provided the diffusion potential $V_{do}$ at the extended defects is large. In the limit of $V_{do} \cong E_g/2q$ with $E_g$ the energy gap, the high-injection condition at the defect ($n \sigma_n \cong p \sigma_p$) occurs at virtually all illumination intensities. High-injection effects for bulk recombination through point defects (as expected in crystalline material) occurs only when $n_v \sigma_n \cong p_v \sigma_p$, which is usually only under concentrated sunlight for extrinsic silicon.[20]

We believe that the above model explains the enhanced spectral response at long wavelengths under optical bias shown in Fig. 3, the absence of these effects in solar cells made from crystalline silicon, and the earlier observations of these effects in ribbon silicon cells. The photoresponse of the polycrystalline Si devices without optical bias, as shown in Fig. 2, is only 25% to 75% of that for the crystalline devices (depending upon $\lambda$) over the

wavelength range of interest. With the optical bias, however, the response of the polycrystalline devices (but not the crystalline devices) is improved. This results in an AM1 short-circuit current density only marginally smaller in the polycrystalline than in the crystalline case. The present explanation does not depend upon assumptions of multi-level centers or trap saturation, but only upon the established presence of space-charge regions surrounding extended defects (dislocations and grain boundaries) in the cast (polycrystalline) and ribbon silicon materials.[21]

It has been determined[16] that for minMIS solar cells on crystalline (Czochralski) silicon fabricated in our laboratory, the short-circuit current density under AM1 conditions is 35 mA $cm^{-2}$ . In identical cells made from Wacker Silso silicon, the short-circuit current density falls only slightly, to 30.5 mA $cm^{-2}$ . This is shown in Fig. 5; compare the characteristics of (a) and (c). Device (b) is of a different type in which the photocurrent is the same as (a), but the dark current is comparable to (c). In cases (a) and (c) the silicon is p-type; in (b) it is n-type and the grating is reacted with the silicon to form a 'peaked' Schottky barrier.[16] The minor reductions in short-circuit current from (a) to (c) are consistent with the beneficial effects of the AM1 optical bias upon the spectral response for the Wacker material alone, allowing it to perform nearly as well as the crystalline silicon which is not affected by the optical bias at this illumination level.

Figure Captions

Fig. 1 Schematic experimental arrangement employed in obtaining results of Fig. 1 (no optical bias $I_{sc} = i_{\lambda}$) and Fig. 3 (with optical bias $I_{sc} = I_{sco} + i_{\lambda}$).

Fig. 2 Spectral response (quantum efficiency) of minMIS solar cells made from p-type Wacker 'Silso' cast polycrystalline silicon, and from crystalline Czochralski silicon. Obtained from short-circuit current measurements.

Fig. 3 Spectral response of minMIS solar cells made from p-type Wacker 'Silso' cast polycrystalline silicon, with the intensity of an optical bias (white light from GE ELH lamp) as a parameter (normalized to result in absence of optical bias, Fig. 2). Obtained from incremental response of short-circuit current to chopped monochromatic light of low intensity.

Fig. 4 Energy-band diagram in neighborhood of extended defect in silicon (a) in equilibrium, and (b) under appreciable optical illumination. Superimposed on these figures is a schematic distribution of trap states, or recombination centers.

Fig. 5 Characteristics of grating solar cells; described in detail in Ref. (16). Note that a modest reduction in short-circuit current is experienced in changing from crystalline to Wacker silicon (curves (a) and (c) respectively).

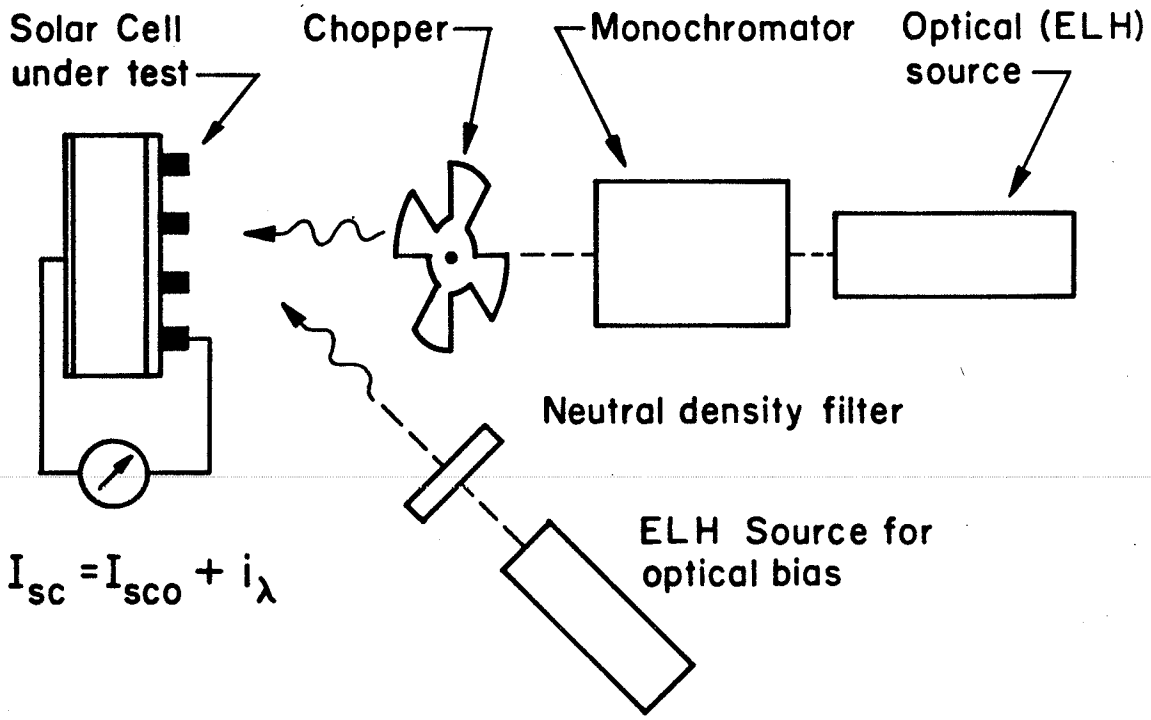
Solar Cell under test
Chopper
Monochromator
Optical (ELH) source
Neutral density filter
ELH Source for optical bias
$I_{sc} = I_{sco} + i_\lambda$

Fig.1

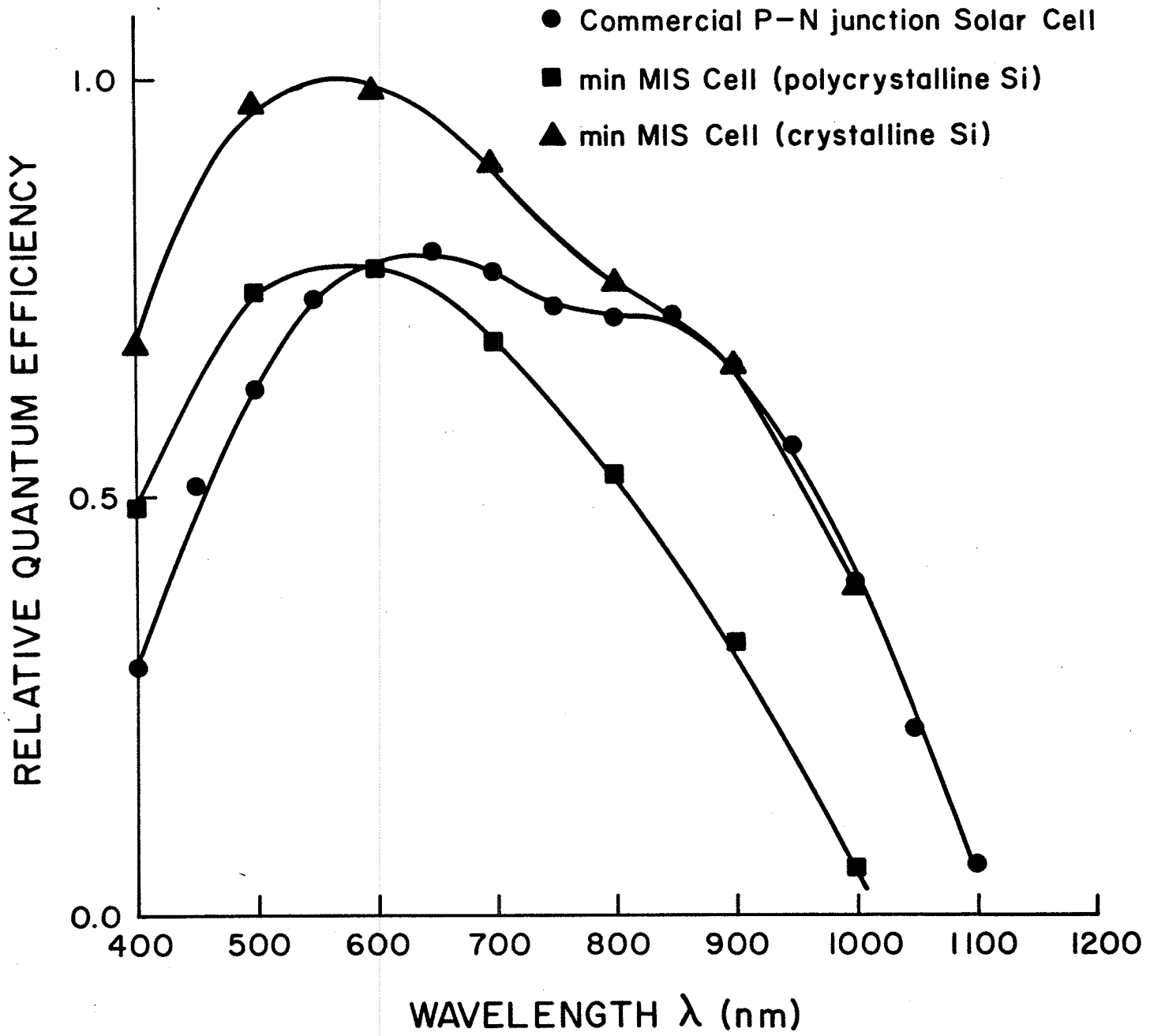
Commercial P–N junction Solar Cell
min MIS Cell (polycrystalline Si)
min MIS Cell (crystalline Si)
RELATIVE QUANTUM EFFICIENCY
1.0
0.5
0.0
400
500
600
700
800
900
1000
1100
1200
WAVELENGTH λ (nm)

Fig. 2

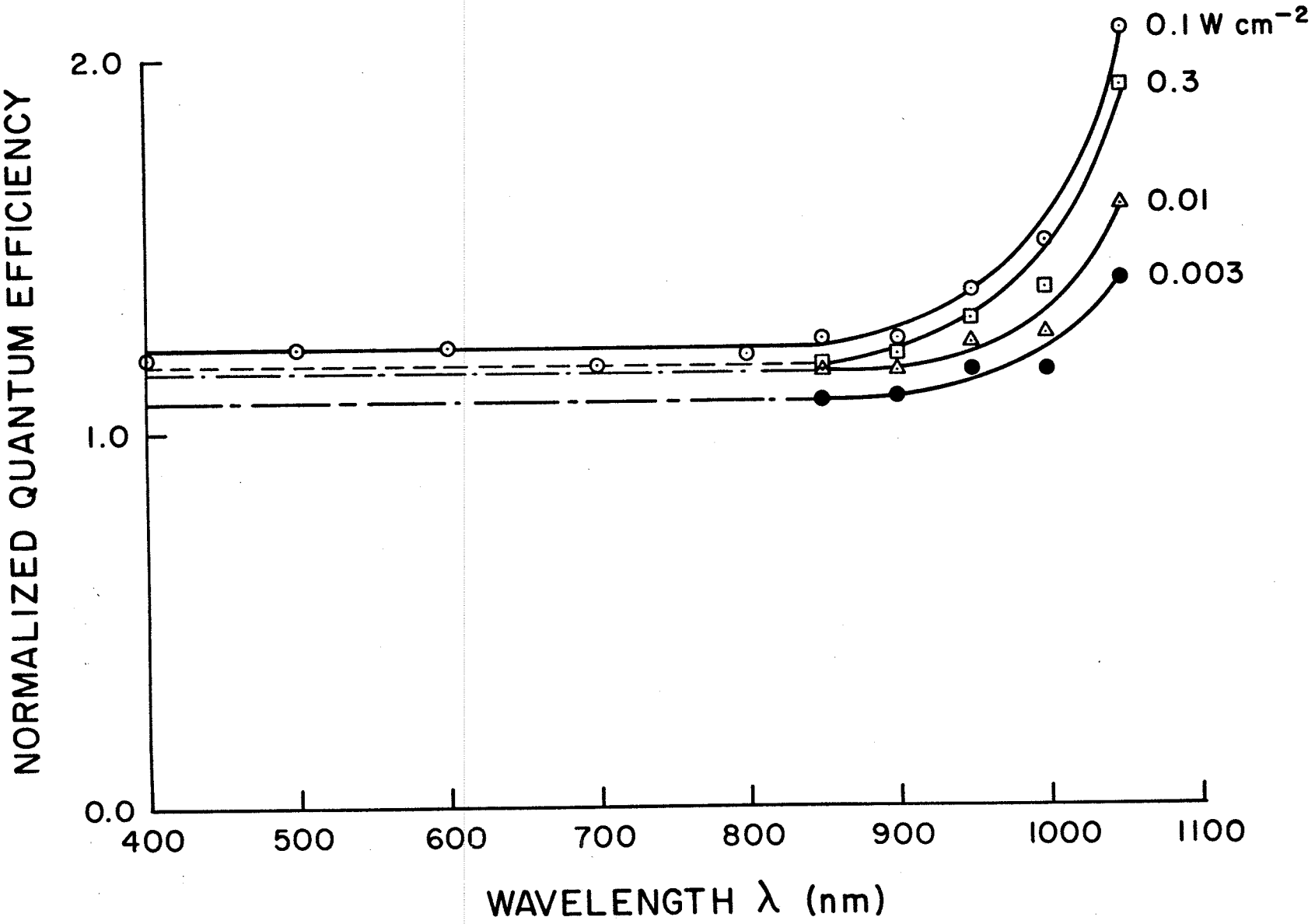
NORMALIZED QUANTUM EFFICIENCY
2.0
1.0
0.0
400
500
600
700
800
900
1000
1100
WAVELENGTH λ (nm)
0.1 W cm$^{-2}$
0.3
0.01
0.003

Fig. 3

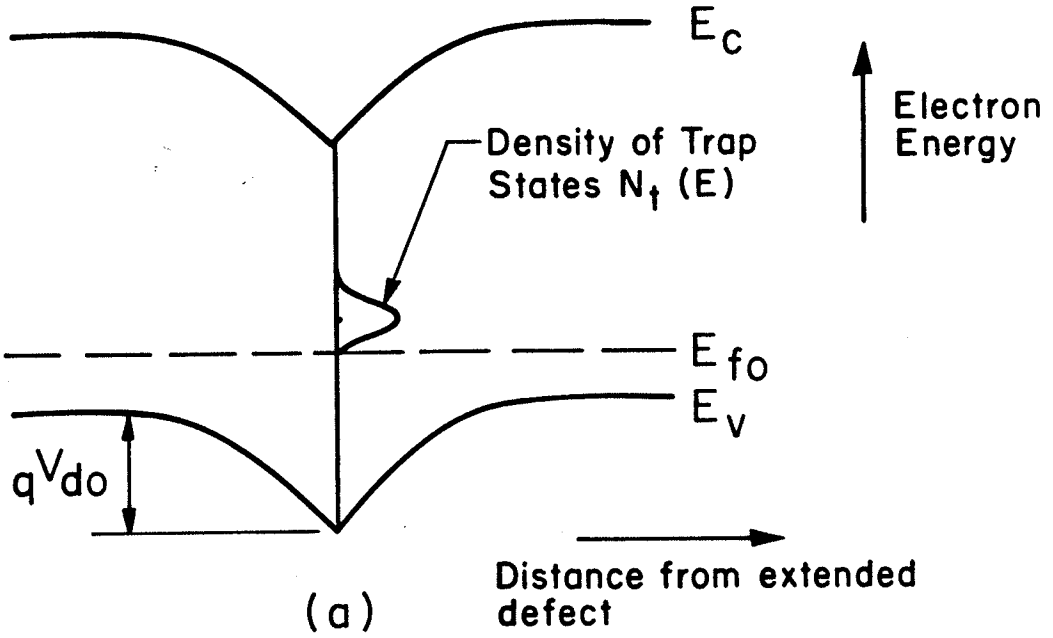
$E_c$
Electron Energy
Density of Trap States $N_t$ (E)
$E_{fo}$
$E_v$
$qV_{do}$
Distance from extended defect

(a)

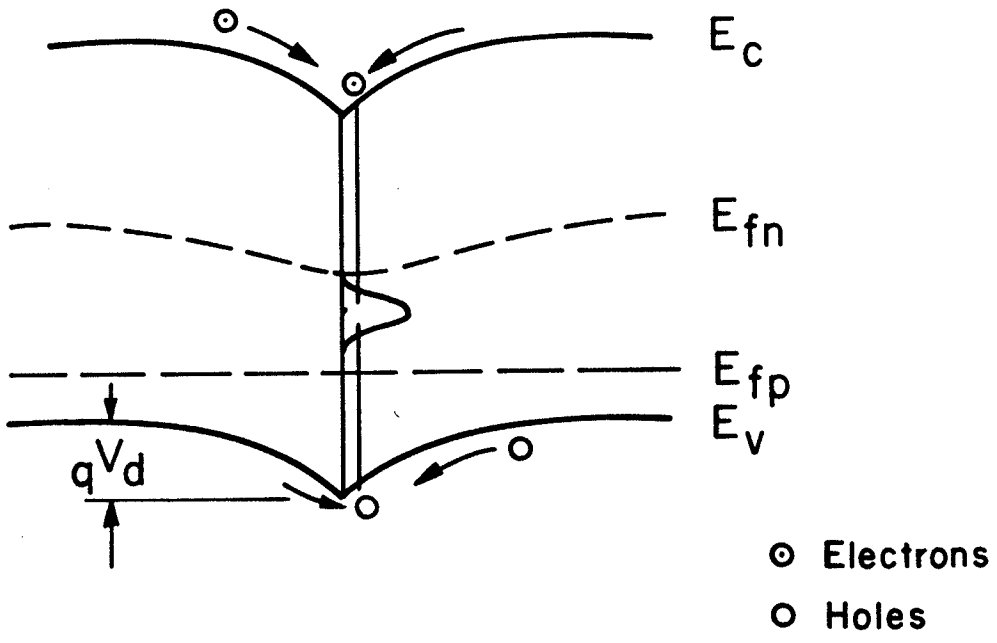
$E_c$
$E_{fn}$
$E_{fp}$
$E_v$
$qV_d$
Electrons
Holes

(b)

Fig. 4

(a) Czochralski Si min MIS Cell $\eta \simeq 14.0\ \%$

(b) Czochralski Si majority current Cell $\eta \simeq 11.4\ \%$

(c) Wacker Silso Si min MIS Cell $\eta \simeq 10.3\ \%$

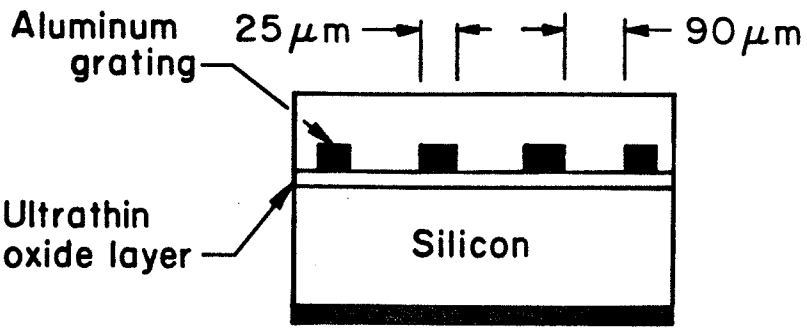


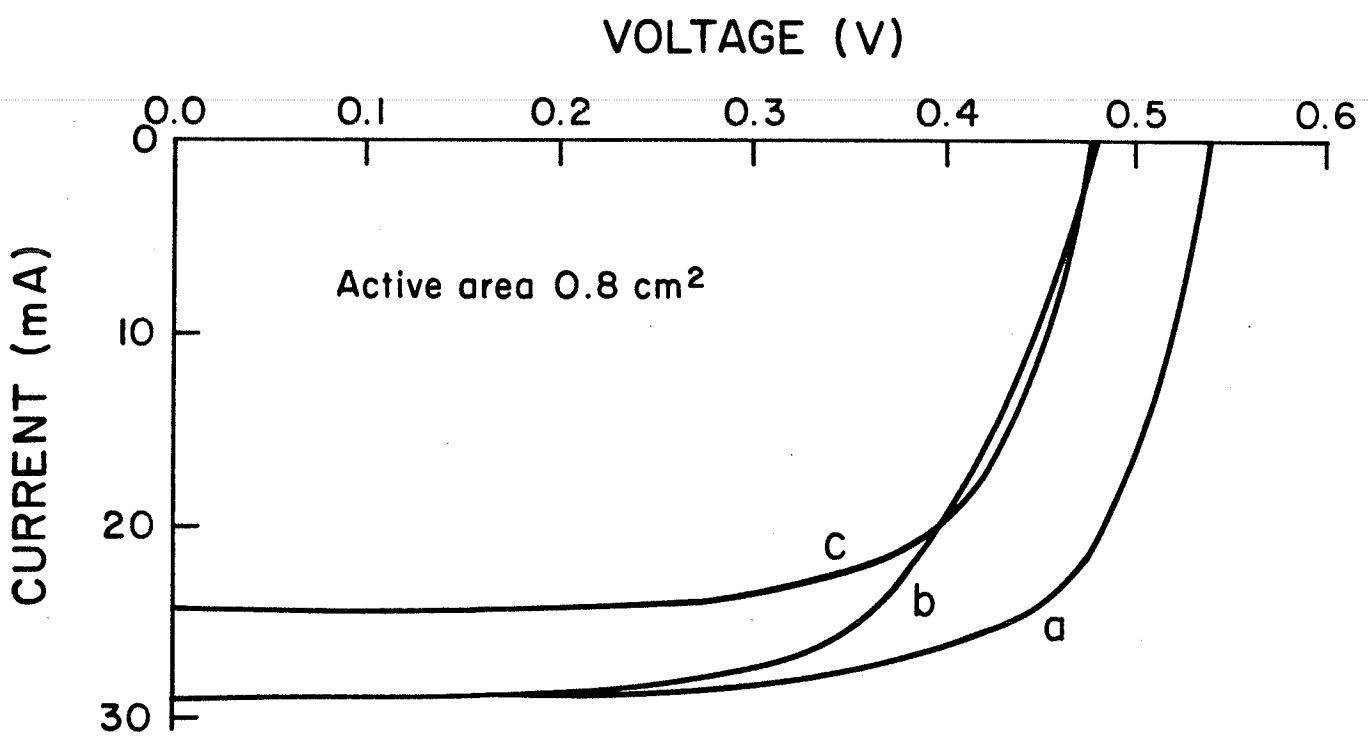


Fig. 5

# CHAPTER III

## A Model of Silicon Solar Cells for Concentrator Photovoltaic and Photovoltaic/Thermal System Design

### 3.1 Synopsis of Solar Cell Properties under Unconcentrated Sunlight (C=1)

In order to begin our discussion of the effects of optical concentration and temperature, it will be helpful to briefly review the photovoltaic properties of solar cells under unconcentrated (1 sun) illumination, in which case the cell can be assumed to be at ambient temperature (C = 1, T = 300K). Fig. 6 shows a schematic diagram of a typical solar cell of a geometry which would be appropriate for concentrator applications. In this thesis, we restrict our attention to silicon solar cells since most commercial cells are made from silicon, although GaAs is another promising semiconductor material for concentrator applications.[40] The basic components of the solar cell in Fig. 6 are the P-N junction in the silicon, which separates the photo-generated carriers and across which the photovoltage is developed when under optical illumination. The metal grid fingers are designed to admit the maximum light without introducing excessive series resistance into the collection process of the photogenerated carriers. The design of this grid generally becomes more involved with increased solar concentration, since for a concentration ratio of 100, for example, the series resistance must be 100 times smaller for the same voltage loss in this resistance. For convenience we have shown the total series resistance (from both top and bottom contacts as well as from the bulk semiconductor) as a lumped 'external' parameter $r_s$ . (Similarly for the 'shunt' resistance $R_{sh}$). The heavily-

doped (p+) region adjacent to the back ohmic contact provides the well-known "back surface field" effect which reduces recombination of the photogenerated carriers and improves the open-circuit voltage.[22-24] The load resistance $R_L$ is ideally chosen for maximum power transfer from the cell; this will of course depend upon the concentration ratio and is of the order of $R_L \cong V_{oc}/I_{sc}$ .

The dark current in the solar cell, $I_d$ , is given to a good approximation, even in imperfect cells, by [43]

$$I_d = I_o [\exp(V_j/V_T) - 1] + I_r[\exp(\frac{V_j}{2V_T}) - 1] \qquad (18)$$

where $V_j$ is the photovoltage developed across the P-N junction only, such that $V_j = V + Ir_s$ with V the total (external) voltage, and $V_T = \frac{kT}{q}$ , and the currents $I_o$ and $I_r$ are given by[43]

$$I_o \cong a \frac{q D n_i^2}{N L} \tanh (d/L)$$

$$\cong a \frac{q n_i^2 d}{N\tau} \quad \text{for} \quad L >> d \qquad (19)$$

$$I_r = a \frac{q n_i W}{2\tau} \qquad (20)$$

with a the junction area, d the width of the base region in Fig. 6, N the doping concentration in this region, D and L, the diffusion coefficient and diffusion length for minority carriers in the base region (electrons in N+PP+ cell and holes in the P+NN+ cell). W is the width

of the junction space-charge region, $\tau$ is the recombination lifetime in this region and $n_i$ is the intrinsic concentration, given for silicon by (33)

$$n_i = 3.9 \times 10^{16} \; T^{3/2} \exp\left(-\frac{E_{go}}{2kT}\right) \tag{21}$$

$E_{go}$ is the 0°K energy gap in silicon (1.21 eV); $n_i$ is in units of $cm^{-3}$.

The photocurrent $I_{ph}$ is given by (22-24, 43, 44)

$$I_{ph} = q\,A \int_0^{hc/E_g} F(\lambda)(1-R(\lambda))Q(\lambda)\; d\lambda \tag{22}$$

where $F(\lambda)$ is the solar flux density per unit wavelength at the wavelength $\lambda$, $R(\lambda)$ is the reflection coefficient from the solar cell surface, and $Q(\lambda)$ is the quantum efficiency for collection of minority carriers photogenerated by photons of wavelength $\lambda$. The useful spectrum cuts off at $\lambda = hc/E_g$, where $E_g$ is the energy gap or minimum photon energy which can be absorbed in the material (1.12 eV for silicon at 300°K).

As we see from Fig. 6(b), the total current flowing in the external load $R_L$ is given by

$$I = I_{ph} - I_d$$

$$= I_{ph} - I_0\left[\exp\left(\frac{V + Ir_s}{V_T}\right) - 1\right] - I_r\left[\exp\left(\frac{V + Ir_s}{2V_T}\right) - 1\right] \tag{23}$$

where V is the voltage across the (external) load resistance $R_L$. The open-circuit voltage $V_{oc}$ is the value of V for which $I = 0$ ($R_L = \infty$) and

is obtained by solving Eqn. (23) for $V$ with $I$ set to zero. The short-circuit current $I_{sc}$ is the value of I in Eqn. (23) for $V = 0$ which is not exactly $I_{ph}$ for $r_s > 0$ .

For moderate values of series resistance ($r_s \leqq V_T/I_{sc}$) we can write for the short-circuit current

$$I_{sc} \cong I_{ph} \tag{24}$$

obtained by setting $V = 0$ in Eqn. (23), and for the open-circuit voltage,

$$V_{oc} \cong V_T \ln\left(\frac{I_{ph}}{I_o}\right) \tag{25}$$

obtained by setting $I = 0$ in Eqn. (23). In arriving at Eqn. (25), we have assumed that $V_{oc} >> V_T$ and furthermore that $V_{oc}$ is sufficiently large that the last term in Eqn. (23) for the recombination current is negligible at this voltage $V = V_{oc}$ . This will be well justified at one sun intensity and above.

For a particular operating point $I,V$ in Fig. 6(c), the power $IV$ will be maximized. At this point we define the fill factor (FF) as $IV/I_{sc}V_{oc}$, so that the photovoltaic efficiency may be written as

$$\eta = \frac{I_{sc}\ V_{oc}\ FF}{P_{opt}} \times 100\% \tag{26}$$

where $P_{opt}$ is the optical power coupled into the cell.

## 3.2 The Effects of Optical Concentration

Under intense optical illumination associated with substantial concentration of the sunlight incident upon the solar cell, a number of complexities arise in the physical operation of the device.[32-42]

For the purpose of arriving at a model for concentrator cells which is useful in system design, we will choose to neglect most of these effects. This restricts the validity of our model somewhat, but for the explanation of silicon solar cells below approximately 200 suns, only minor compromises in accuracy are made. This is partially a property of the relatively large base doping concentrations of concentrator cells.[22-24,43,44] The justification of this approach will be the satisfactory agreement of the model predictions with available experimental data as described later.

The major factor contributing to the possibility of degraded performance at high solar concentration (C) is the presence of internal series resistance ($r_s$) . This becomes increasingly problematic at large C because the photocurrent increases linearly with C whereas the photovoltage increases only logarithmically with C. (see below). Disregarding the small increases in voltage with C, it is therefore apparent that when C is doubled, the tolerable $r_s$ must be approximately halved. As a rough guide, the maximum series resistance allowed could be specified as $0.1\ V_{oc}/I_{sc}$ . Since for C = 1, $V_{oc} \cong 0.6V$ and $I_{sc} \cong 0.03$ A per cm² of cell area, we have that

$$r_{s_{(max)}} \cong \frac{2}{aC} \qquad (27)$$

with $r_s$ in ohms and a in $cm^2$ as the (active) cell area, in order to avoid

catastrophic degradation of the photovoltaic performance. At a solar concentration factor of $C = 10$, for example, the maximum allowed $r_s \cong 0.2\ \Omega$ for a 1 $cm^2$ solar cell.

The shunt resistance $R_{sh}$ is generally sufficiently large in carefully prepared solar cells so as not to be of concern, and this is a problem which is diminished under conditions of optical concentration.

The photocurrent can be calculated using Eqn. (22) for the known solar spectrum,[22] or alternatively one can obtain the appropriate values by recourse to experimental data under air-mass one (AM1) conditions. For solar cells of the geometry used in concentrator applications (P+NN+ or N+PP+ cells as shown schematically in Fig. 6), the short-circuit photocurrents at 300K are experimentally observed to be 0.034 A per $cm^2$ for one sun illumination, within approximately ±5% for devices from several laboratories.[27-31] Under concentration C, we therefore employ the simple relationship, valid for T = 300K,

$$I_{sc} \cong 0.034\ a\ C \tag{28}$$

where $a$ is the active (photosensitive) area of the solar cell.

There will be a modest correction to $I_{sc}$ in the presence of excessive series resistance ($r_s$ in Eqn. (6)) but this may be ignored since the effects of $r_s$ on fill-factor (FF) are much greater. This will be disscussed later in this section.

The open-circuit voltage is obtained from Eqn. (25) with the relation $I_{ph} \cong I_{sc} \cong 0.034\ a\ C$ from (28).

$$V_{oc} \cong V_T \ln\left(\frac{0.034\ a\ C}{I_o}\right)$$

$$= 8.7 \times 10^{-5}\ T\ \ln\left(\frac{0.034\ a\ C}{I_o}\right) \qquad (29)$$

where $V_T = kT/q = 8.7 \times 10^{-5}\ T$ has been entered into the second form. We also have, for the dark saturation current of the pn junction, that

$$I_o \cong 1.5 \times 10^{-12}\ a\left(\frac{T}{300}\right)^3 \exp\left[7.1 \times 10^3 \left(\frac{1}{300} - \frac{1}{T}\right)\right] \qquad (30)$$

with the value $1.5 \times 10^{-12}$ A $cm^{-2}$ adopted as an average experimental result at 300K[27-31] and the temperature dependence arising from the $n_i^2$ term in Eqn. (19), according to Eqn. (21). The value $7.1 \times 10^3$ has been calculated for $E_{go}/2k$ in (21) as appropriate to the OK energy gap in silicon of $E_{go} = 1.21$ eV.

At T = 300 K, the dependence of the open-circuit voltage upon optical concentration may be written as

$$\begin{aligned} V_{oc} &\cong 0.026\ \ln(2.27 \times 10^{10}\ C) \\ &= 0.62 + 0.026\ \ln C \\ &= 0.62 + 0.06\ \log_{10} C \end{aligned} \qquad (31)$$

There is actually a dependence of the first term in (31) upon the base doping concentration of the solar cell (N in Eqn. (19)). This could be included in the model for accuracy, but in order to maintain a small number of parameters (C and T alone) we sacrifice this additional accuracy. Actually the sacrifice is not great, since the base dopings in solar cells which have been optimized for concentrator applications will not differ appreciably among devices from various sources.

The temperature dependence of $V_{oc}$ is contained in the factors $T$ and $I_o$ of Eqn. (29) with the $T$ dependence of $I_o$ given by (30). An explicit $V_{oc}(T)$ expression by this approach is rather awkward. We have found empirically that $dV_{oc}/dT \cong (V_{oc} - 1.25)/300$ where the $V_{oc}$ on the right refers to 300K value given by Eqn. (31). Combining this result with (31) leads to

$$V_{oc} \cong 1.25 - \left(\frac{0.63 - 0.06 \log_{10} C}{300}\right) T \qquad (32)$$

The temperature dependence of the short-circuit current arises primarily because the cutoff wavelength $\lambda = hc/E_g$ in Eqn. (22) for the photocurrent increases with temperature. This is because the energy gap of the silicon $E_g$ decreases with temperature.[42] The effect on $I_{ph}$, i.e. on $I_{sc}$, of the increased optical absorption is complicated by the dependence of the collection efficiency for the photogenerated carriers (Q in Eqn. (22)) on $\lambda$. We refer instead to the results of Hall[42] that the temperature coefficient of the short-circuit current in silicon $(1/I_{sc})(dI_{sc}/dT) = 3 \times 10^{-4}\ K^{-1}$, so that we can write

$$I_{sc} = 0.034\ a\ C\ (1 + 3 \times 10^{-4}(T-300)) \qquad (33)$$

An expression for the current-voltage characteristics under conditions of optical concentration, which is more convenient than Eqn. (23), is obtained by removing the quantity $I_o$ and replacing it with a $V_{oc}$ dependence. From (23),

$$I \cong I_{sc}\left(1 - \frac{I_o}{I_{sc}} \exp\left(\frac{V + I r_s}{V_T}\right)\right)$$

$$\cong I_{sc}\left(1 - \exp\left(-\frac{V_{oc}}{V_T}\right) \exp\left(\frac{V + I r_s}{V_T}\right)\right)$$

$$\cong I_{sc}\left(1 - \exp\left(\frac{V + I r_s - V_{oc}}{8.7 \times 10^{-5} T}\right)\right) \qquad (34)$$

where Eqns. (24) and (25) were used, and $I_r$ in (33) has been assumed to be negligible (ideal junction). We have also used $V_T = kT/q = 8.7 \times 10^{-5} T$.

The fill factor may be determined for any operating condition (C and T) by finding the maximum power point at which

$$\frac{dP}{dV} = \frac{d}{dV}(IV) = 0 \qquad (35)$$

with I(V, C, T) given by (34) with substitutions from Eqns. (32) and (33). Solving (35) for $V = V_m$ and substituting $V_m$ in (34) to obtain $I_m$, the fill factor is then given by $V_m I_m / V_{oc} I_{sc}$ as discussed earlier. A simple and sufficiently accurate expression for the fill factor has been obtained by Green[45]

$$FF \cong \frac{\left[\frac{V_c}{V_T} - \ln\left(\frac{V_{oc}}{V_T} + 0.72\right)\right]\left(1 - \frac{I_{sc} r_s}{V_{oc}}\right)}{\frac{V_{oc}}{V_T} + 1} \qquad (36)$$

We further simplify this expression by taking advantage of the experimental observation that for small $r_s$, FF may be satisfactorily described by the empirical expression $0.8 - 0.0006\,(T-300)$. We also find that an

average value of $V_{oc}$ over the range of C and T of interest, of 0.7 V may be used in the last term of the numerator in Eqn. (36) to arrive at

$$FF \cong [0.8 - 0.0006\ (T - 300)]\ (1 - 0.05\ C\ a\ r_s) \qquad (37)$$

The dependence of the photovoltaic conversion efficiency on C and T may now be expressed as

$$\eta = \frac{I_{sc}\ V_{oc} FF}{0.1\ a\ C} \times 100\% \qquad (38)$$

with $V_{oc}$ (C, T), $I_{sc}$ (C, T) and FF(C, T) given by Eqns. (32), (33) and (37) respectively. Eqn. (38) is a restatement of Eqn. (26) with $P_{opt} = 0.1\ a\ C$ in watts for the optical power from concentrated solar illumination with an AM1 spectrum.[22-24]

Expression (38) describes the conversion efficiency at the operating voltage for maximum power. This maximum power point is dependent upon C and T. In photovoltaic system design, all solar cells may not be operating at their maximum power points, for example when they are interconnected in a module in which C and/or T is not the same for all cells. In this case we must return to Eqn. (34) in order to establish the conversion efficiency at the (non-optimal) operating voltage. In these cases, Eqn. (38) is replaced by

$$\eta = \frac{I\ V}{0.1\ a\ C} \times 100\% \qquad (39)$$

where I is obtained from Eqn. (34) for the appropriate operating conditions of V, C and T, with $V_{oc}$ and $I_{sc}$ expressed by (32) and (33).

Table 2 summarizes the model in its most convenient form for application to the design of concentrator photovoltaic systems.

## 3.3 Comparison with Experimental Data

In this section we compare the photovoltaic parameters calculated from our simplified expressions with available experimental results from several laboratories. It should be noted that arbitrarily good agreement could be obtained by more complicated models which took account of variations between devices in geometry, doping concentrations, etc. We wish instead to provide a simple universal model for concentrator solar cells, so that we do not distinguish between the experimental comparisons with the various devices.

Fig. 7 shows the comparison of Eqn. (31) for the open-circuit voltage with experimental data. Although a considerable range of device geometry and doping profiles is encompassed in this data, the agreement with Eqn. (32) for $V_{oc}$ is within 10% in most cases up to an optical concentration of C = 200 or so. In Fig. 8 we show the results for the temperature coefficient of $V_{oc}$, or $dV_{oc}/dT$. It is important to recognize that the differences between the data and the model predictions obtained by differentiating Eqn. (32) translate into very small percentage errors in the estimation of $V_{oc}$ itself at a particular temperature, as a result of the small magnitude of $dV_{oc}/dT$.

It is difficult to obtain experimental data for the short-circuit current $I_{sc}$ vs concentration C because of the common experimental practice of using

$I_{sc}$ to determine the value of $C$. In cases where the solar intensity is independently measured, $I_{sc}$ is found to be approximately linearly dependent upon $C$ except at extremely large optical concentrations $C \gtrsim 500$.[30] For lower $C$, Eqn. (33) is accurate within approximately 5% for virtually all well-designed devices.

The fill-factor (FF) shows appreciable variation among experimental devices at high optical concentrations ($C \gtrsim 50$), as shown in Fig. 9. This arises from variations in series resistance $r_s$. If $r_s$ is treated as an adjustable parameter, Eqn. (37) is accurate within approximately 5% in predicting the experimental data up to 200 suns (Fig. 9).

The photovoltaic conversion efficiency $\eta$ from Eqn. (35), with $V_{oc}$, $I_{sc}$, and FF from (32), (33) and (37) respectively, is shown in Fig. 10. The temperature coefficient of $\eta$, given by

$$\frac{d\eta}{dT} = \eta\left[\frac{1}{V_{oc}}\frac{dV_{oc}}{dT} + \frac{1}{I_{sc}}\frac{dI_{sc}}{dT} + \frac{1}{FF}\frac{d(FF)}{dT}\right]$$

is obtained in turn by differentiating these same equations. $d\eta/dT$ is shown in Fig. 11. Comparison of $\eta$ and $d\eta/dT$ with experimental data in Figs. 10 and 11 indicates that the photovoltaic conversion efficiency at an arbitrary temperature and optical concentration ($C < 200$) is predicted by the present model with an error of less than 15%. For the higher performance concentrator cells in Fig. 10, which will more faithfully represent future devices, the errors in using Eqns. (38), (32), (33) and (37) to determine $\eta$ are less than 5%. This means that the efficiency may be specified as $\eta = (18 \pm 1)\%$, $(20 \pm 1)\%$, etc. depending on $C$ and T,

where the 18, 20, etc. are the predictions of the present model.

In many cases, graphical representations of the model may be preferred to the analytical expressions of Table 2. These are presented in Figs. 12-16. Fig. 12 shows examples of the predicted current-voltage characteristics. Figs. 13-16 present $I_{sc}$, $V_{oc}$, FF and $\eta$ for the range of series resistance $r_s$, operating temperature $T$, and the useful range of concentration $C$. Inaccuracies are to be expected above an optical concentration of approximately $C = 200$; below this $C$ we expect all results of the model to be within 10% of the actual values.

## 3.4 Example of Application of the Model to Design of Concentrator PV and PV/T Systems

Since solar cells produce small voltages (typically 0.6 - 0.8V in concentrator systems), most applications require several cells connected in series. The most cost-effective way of cooling these cells is normally a series-flow arrangement, as shown in Fig. 17. In most applications, parallel-cooling requires excessive pumping power.

For a fixed concentration ratio, $C$, the series cooling requires the cells near the coolant outlet to operate at a higher temperature than cells closer to the inlet, because of the increasing coolant temperature. Also, due to fluid entrance effects, the convective heat transfer coefficient, h, at the location of the first few cells will be considerably higher than at the location of the other cells. The higher temperature cells will produce less power than the lower temperature cells. Since they are connected electrically in series, however, the currents must all be equal.

For fully-developed turbulent flow in a channel, the following correlation [46, 47] can be used to obtain $h(W\ m^{-2}\ K^{-1})$:

$$Nu = 0.023\ R_e^{0.8} P_r^{0.3} \tag{40}$$

The Nusselt number, $Nu$, is given by $\frac{hD}{k}$, where $D$ is the hydraulic diameter of the flow channel $(\frac{4 \times \text{cross-sectional area}}{\text{wetted perimeter}})$ (m), and $k$ is the thermal conductivity of the coolant $(\frac{W}{m\ K})$. The Reynolds number, $Re$, is given by $\frac{VD}{\nu}$, where $V$ is the coolant velocity (m/s), and $\nu$ is the kinematic viscosity of the coolant ($m^2/s$). The Prandtl number, $P_r$, is given by $\frac{C_p\ \rho\ \nu}{k}$, where $C_p$ is the specific heat of the coolant $(\frac{J}{kg\ K})$, and $\rho$ is the density of the coolant ($kg/m^3$). $V$ will be limited by the allowable system pressure drop which is determined by the affordable pumping power.

Equation (40) can be used for cell locations where fully-developed turbulent flow is present. However, for cells near the inlet, fluid entrance effects must be taken into account. If the ratio of distance from the inlet, $L$, to hydraulic diameter, $D$, is between 10 and 400, the following correlation [46,47] can be used:

$$Nu = 0.036\ R_e^{0.8} P_r^{1/3} \left(\frac{D}{L}\right)^{0.055} \tag{41}$$

Kreith [48] recommends the following correlation for short tubes with abrupt contraction entrances:

$$\frac{h_L}{h_\infty} = 1 + \left(\frac{D}{L}\right)^{0.7} \qquad (42)$$

$$\text{if } 2 < \frac{L}{D} < 20 ,$$

and

$$\frac{h_L}{h_\infty} = 1 + 6\,\frac{D}{L} , \qquad (43)$$

$$\text{if } \frac{L}{D} > 20 .$$

where $h_\infty$ is the heat transfer coefficient for an infinitely long tube.

The h values obtained from Eqns. (40) to (43) will be sufficiently accurate for most PV/T applications. Non-uniform heat fluxes around the channel perimeter and along the length would have to be taken into account to obtain more accurate h values.[49,50]

The temperature drop across the interlayer between the cells and channel can be calculated from the equation:

$$\Delta T = \frac{q'' x}{k} \qquad (44)$$

where q" is the local heat flux $\left(\frac{W}{m^2}\right)$, x is the thickness of the interlayer (m) and k is the thernal conductivity of the interlayer $\left(\frac{W}{m\,K}\right)$.

The temperature difference between the channel wall and the fluid is given by:

$$\Delta T = \frac{q''}{h} \quad . \tag{45}$$

Therefore, for a given coolant, channel geometry, coolant inlet temperature, coolant velocity, cell spacing, local heat flux, and interlayer material, the temperature of each cell can be calculated from equations (40) to (45).

For a given cell area (a), concentration ratio (C), series resistance ($r_s$), and cell temperature (T), the current for each cell can be calculated as a function of the cell voltage, $I_1(V_1)$, $I_2(V_2)$, ... $I_n(V_n)$, from equations (32) to (34).

Since the currents must all be equal, one can equate these functions:

$$I = I_1(V_1) = I_2(V_2) = I_n(V_n) \tag{46}$$

and obtain each of the voltages $V_2, V_3, \ldots, V_n$, as a function of $V_1$. The total power of the array is:

$$P_T = I(V_1 + V_2 + \ldots + V_n) \tag{47}$$

Each of the voltages and currents are functions of $V_1$. One can then obtain the optimum $V_1$ by setting $\frac{dP_T}{dV_1} = 0$. Equation (47) will now give the maximum total power of the array for a given coolant flow rate.

For the case of a concentrator photovoltaic array, (thermal energy not used), the load resistance is the system variable and the maximum total array power point may be found with the above procedure. In a photovoltaic/thermal (PV/T) system, the inlet temperature or velocity of the coolant is the variable; pumping costs must be evaluated, and the maximum system power point may be obtained in a similar fashion. The thermal application will require a certain range of outlet coolant temperature, which will impose additional constraints on the above optimization procedure.

TABLE 2

Photovoltaic Parameters vs. Optical Concentration Ratio C , Operating Temperature T (K), Cell Area a ($cm^2$) and internal series resistance $r_s$ (ohms). $I = V/R_L$ for load $R_L$ (ohms).

Current-voltage characteristics

$$I = I_{sc}[1 - \exp(\frac{V + 1r_s - V_{oc}}{8.7 \times 10^{-5} T})] \qquad \text{(amps)}$$

Short-circuit current

$$I_{sc} = 0.034\ a\ C\ [1 + 3 \times 10^{-4}\ (T - 300)] \qquad \text{(amps)}$$

Open-circuit voltage

$$V_{oc} = 1.25 - (\frac{0.63 - 0.06\ \log_{10} C}{300})\ T \qquad \text{(volts)}$$

Fill-factor

$$FF = [0.8 - 0.0006(T - 300)](1 - 0.05\ C\ a\ r_s) \qquad \text{(dimensionless)}$$

Conversion efficiency (at optimum load $R_L$)

$$\eta = \frac{I_{sc}\ V_{oc}\ FF}{a\ C\ (0.1)} \times 100\% \qquad (\%)$$

Converstion efficiency (arbitrary load $R_L$)

$$\eta = \frac{I\ V}{a\ C\ (0.1)} \times 100\%$$

For $T = 300K$ , $r_s = 0$

$$I = 0.034\ a\ C\left[1 - \exp\left(\frac{V - V_{oc}}{0.026}\right)\right]$$

$$I_{sc} = 0.034\ a\ C$$

$$V_{oc} = 0.62 + 0.06\ \log_{10} C$$

$$FF = 0.8$$

$$\eta = 0.27\ (0.62 + 0.06\ \log_{10} C) \times 100\%$$

$$= (0.17 + 0.016\ \log_{10} C) \times 100\%$$

for optimum load $R_L$

Figure Captions

Fig. 6 (a) Schematic diagram of N+PP+ solar cell. Distributed series resistance $r_s$ and shunt resistance $R_{sh}$ are treated as lumped 'external' parameters. AR is anti-reflection coating.

(b) Equivalent circuit of solar cell. $I_d$ is dark current. $I_{ph}$ is photocurrent $V_j$ is junction voltage which is larger than V if $r_s$ is significant. $R_{sh}$ can usually be neglected.

(c) Current-voltage characteristics of solar cell showing short-circuit current $I_{sc}$, open-circuit voltage $V_{oc}$ and typical operating point (determined by load $R_L$).

Fig. 7 Open-circuit voltage vs optical concentration according to Eqn. (32) for T = 300K. Comparison with experimental data of Khemthong et al[36] for N+PP+ cells (0.4 Ω cm base resistivity)● and P+NN+ cells (0.4 Ω cm)○; Sanderson and Backus[31] P+NN+ (0.3 Ω cm)■. N+PP+ (0.15 Ω cm and 0.4 Ω cm)□ and N+PP+ (1.5 Ω cm)◆; Nasby et al[30] P+NN+ (0.3 Ω cm) ▲ Frank et al[29] P+NN+ (10-15 Ω cm)▽. C = 1 corresponds to 1 sun (air mass one (AM1), or 100 mW $cm^{-2}$).

Fig. 8 Temperature coefficient of open-circuit voltage vs optical concentration obtained from Eqn. (32) by differentiation. Comparison with experimental data from sources listed in caption to Fig. 7.

Fig. 9 Fill factor vs. optical concentration for T = 300K, with cell area-series resistance product as parameter; obtained from Eqn. (37). Compared with experimental results from sources in Fig. 7.

Fig. 10 Photovoltaic conversion efficiency at $T = 300K$ from Eqns. (32), (33), (37), and (38). Comparison is made with experimental data from sources in Fig. 7.

Fig. 11 Temperature coefficient of photovoltaic conversion efficiency from model predictions; comparison with experimental data from sources in caption to Fig. 7.

Fig. 12 Sample calculations of current-voltage characteristics of silicon concentrator solar cells under various conditions of optical concentration $C$ and temperature $T$.

Fig. 13 Short-circuit current $I_{sc}$ and open-circuit voltage $V_{oc}$ vs. optical concentration with temperature as parameter.

Fig. 14 Fill factor vs. concentration at $T = 300K$ with cell area-series resistance product as parameter. At other temperatures shape is similar but initial value ($C=1$) depends upon $T$ as shown.

Fig. 15 Photovoltaic conversion efficiency vs. optical concentration and temperature. Series resistance assumed negligible in this calculation.

Fig. 16 Photovoltaic conversion efficiency vs. optical concentration at $T = 300K$ with cell area-series resistance product as parameter.

Fig. 17 In design of concentrator photovoltaic/thermal systems such as this one, design decisions (such as coolant flow rates) are facilitated by simple solar cell models.

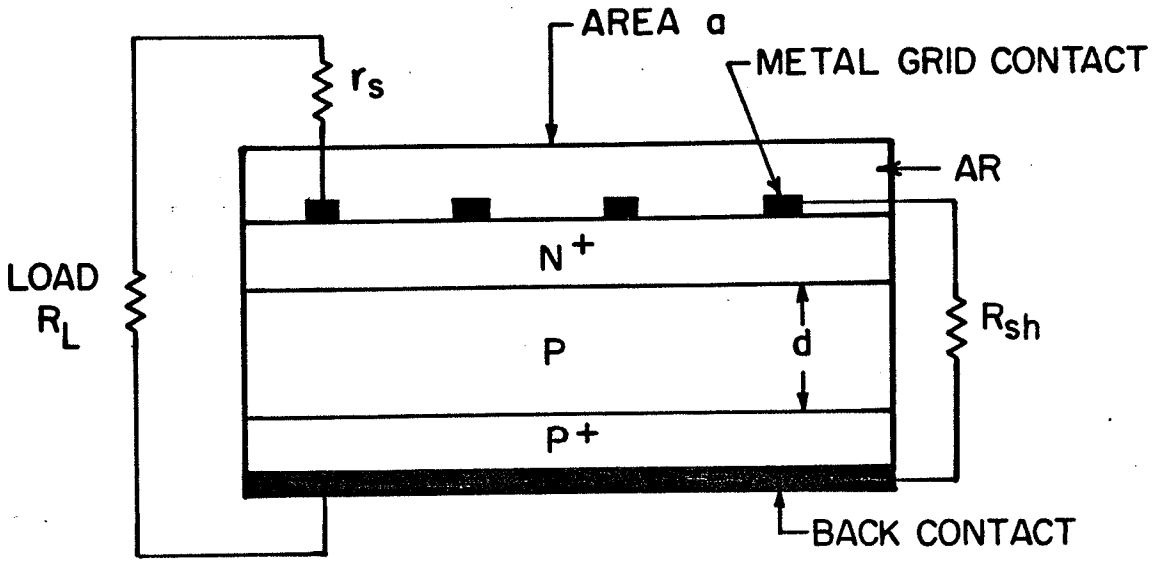


(a)

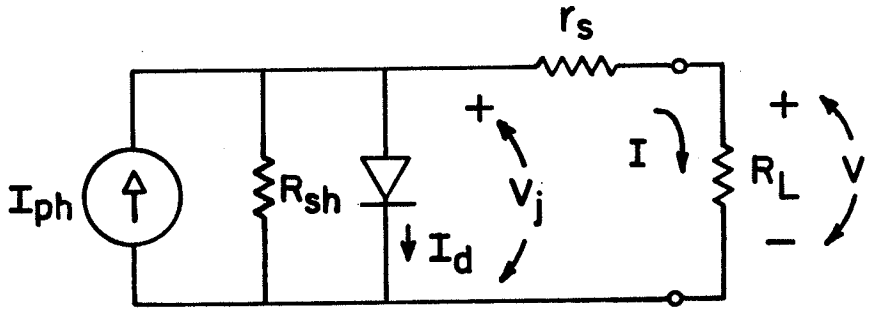


$V_j = V + Ir_s$

$I = I_{ph} - I_d$

(b)

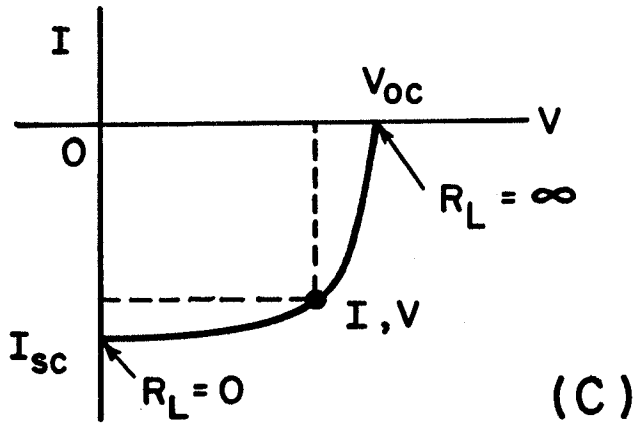


(C)

Fig. 6

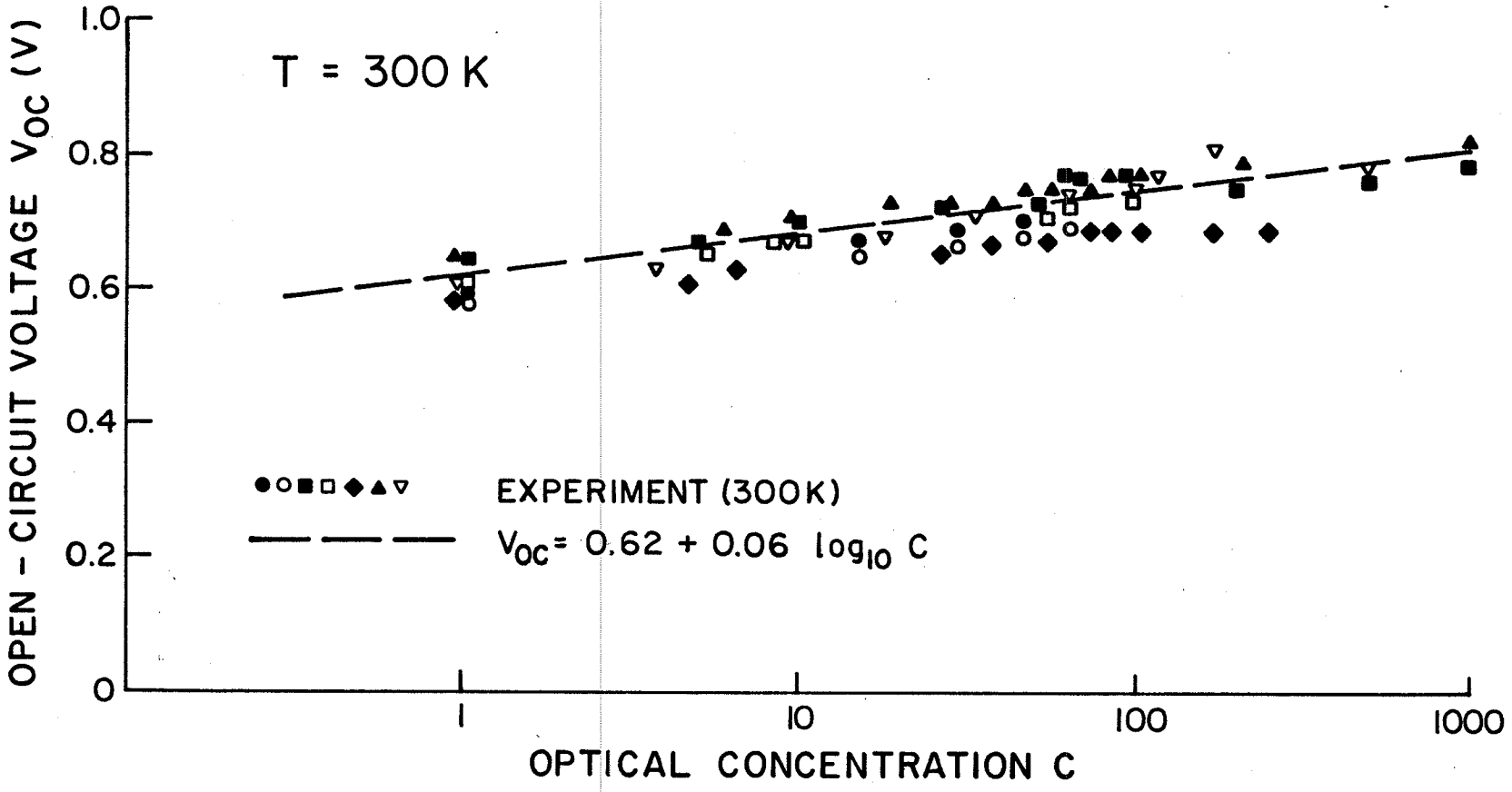
T = 300 K
OPEN - CIRCUIT VOLTAGE $V_{OC}$ (V)
1.0
0.8
0.6
0.4
0.2
0
1
10
100
1000
OPTICAL CONCENTRATION C
EXPERIMENT (300K)
$V_{OC}$ = 0.62 + 0.06 $\log_{10}$ C

Fig. 7

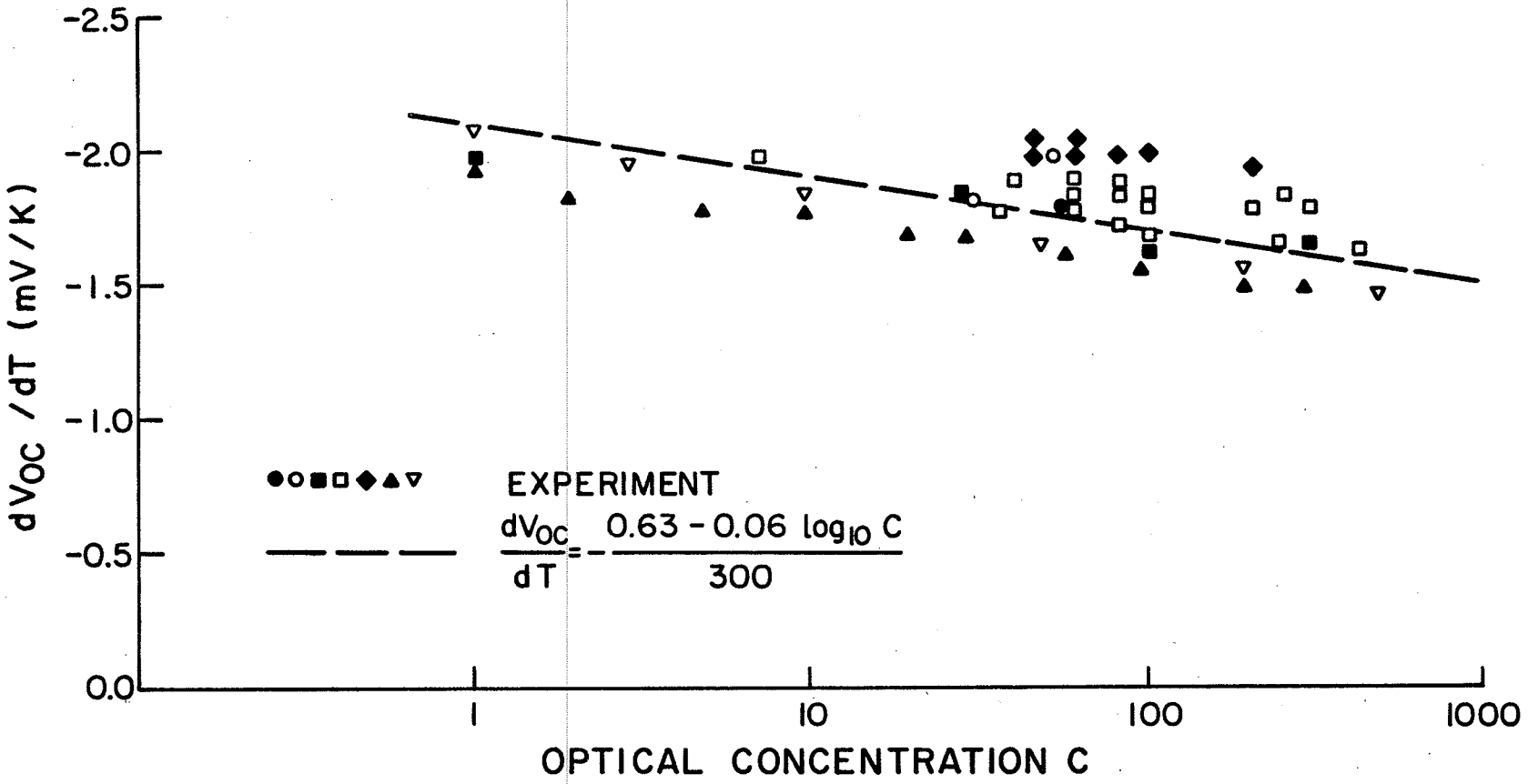
-2.5
-2.0
-1.5
-1.0
-0.5
0.0
dVOC /dT (mV/K)
EXPERIMENT
dVOC/dT = -(0.63 - 0.06 log10 C)/300
1
10
100
1000
OPTICAL CONCENTRATION C

Fig. 8

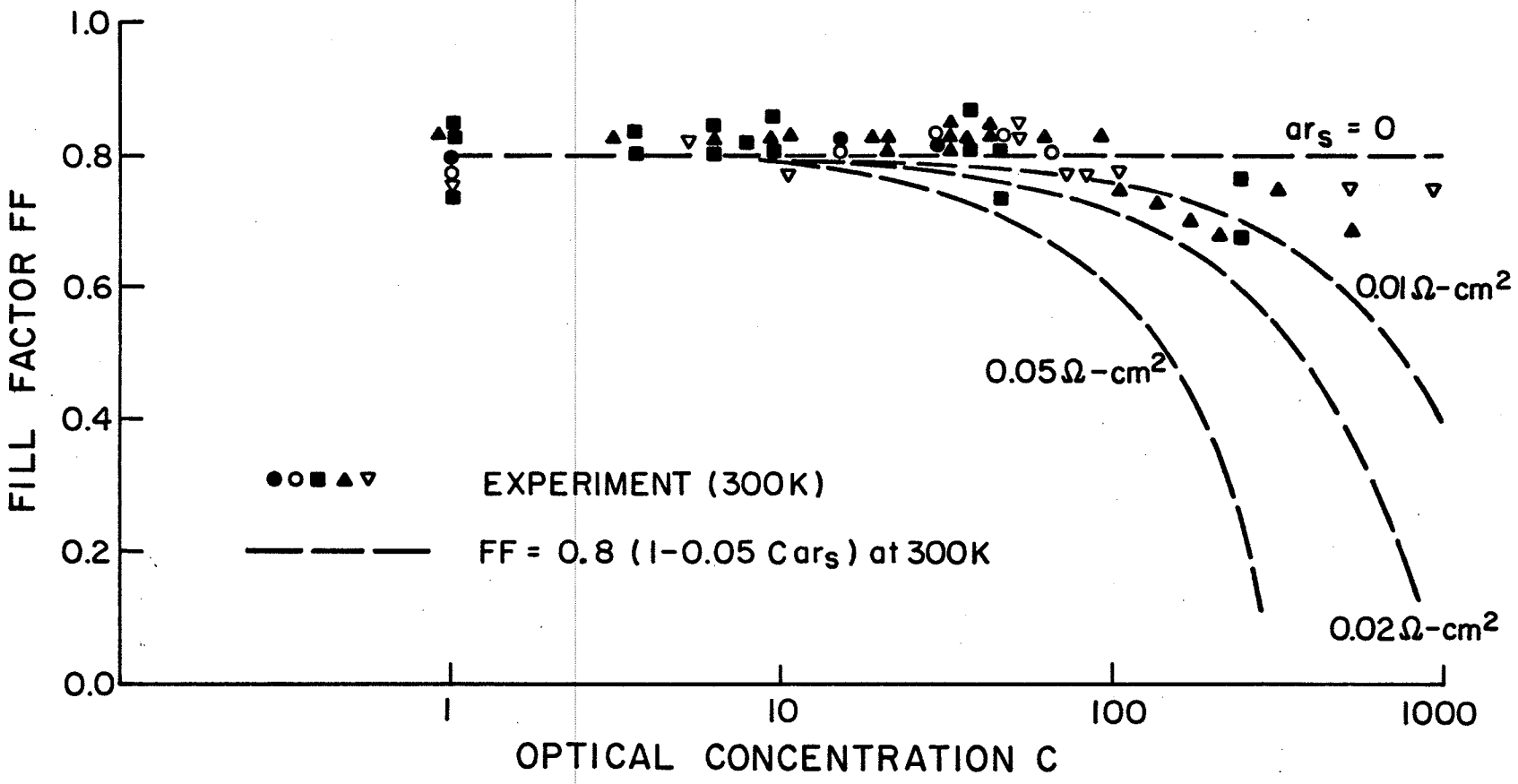
1.0
0.8
0.6
0.4
0.2
0.0
FILL FACTOR FF
$ar_s = 0$
0.01 Ω-cm²
0.05 Ω-cm²
0.02 Ω-cm²
EXPERIMENT (300K)
FF = 0.8 (1-0.05 C$ar_s$) at 300K
1
10
100
1000
OPTICAL CONCENTRATION C

Fig. 9

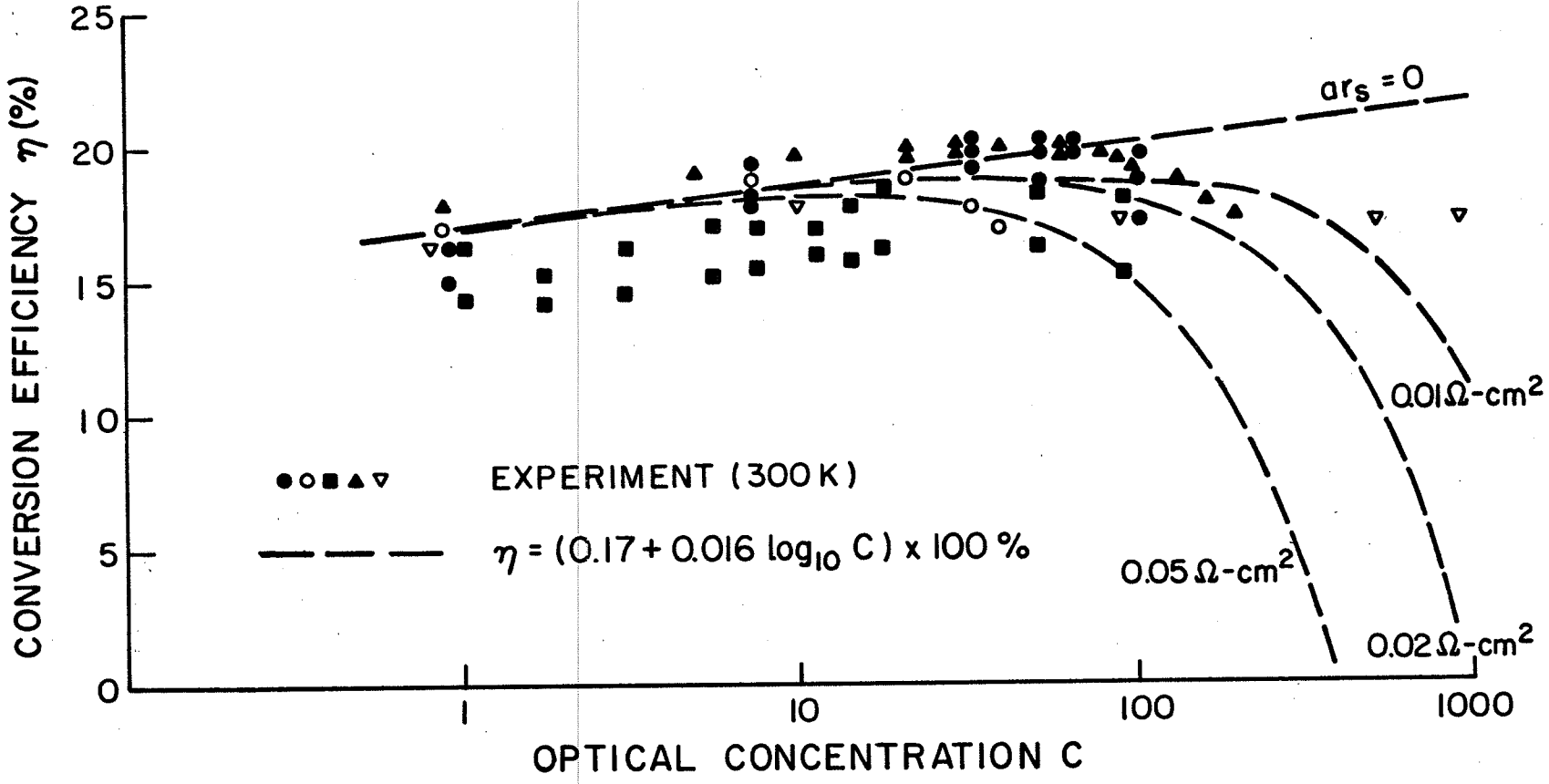
CONVERSION EFFICIENCY η (%)
25
20
15
10
5
0
1
10
100
1000
OPTICAL CONCENTRATION C
$ar_s = 0$
0.01Ω-cm²
0.05Ω-cm²
0.02Ω-cm²
EXPERIMENT (300 K)
$\eta = (0.17 + 0.016 \log_{10} C) \times 100\ \%$

Fig. 10

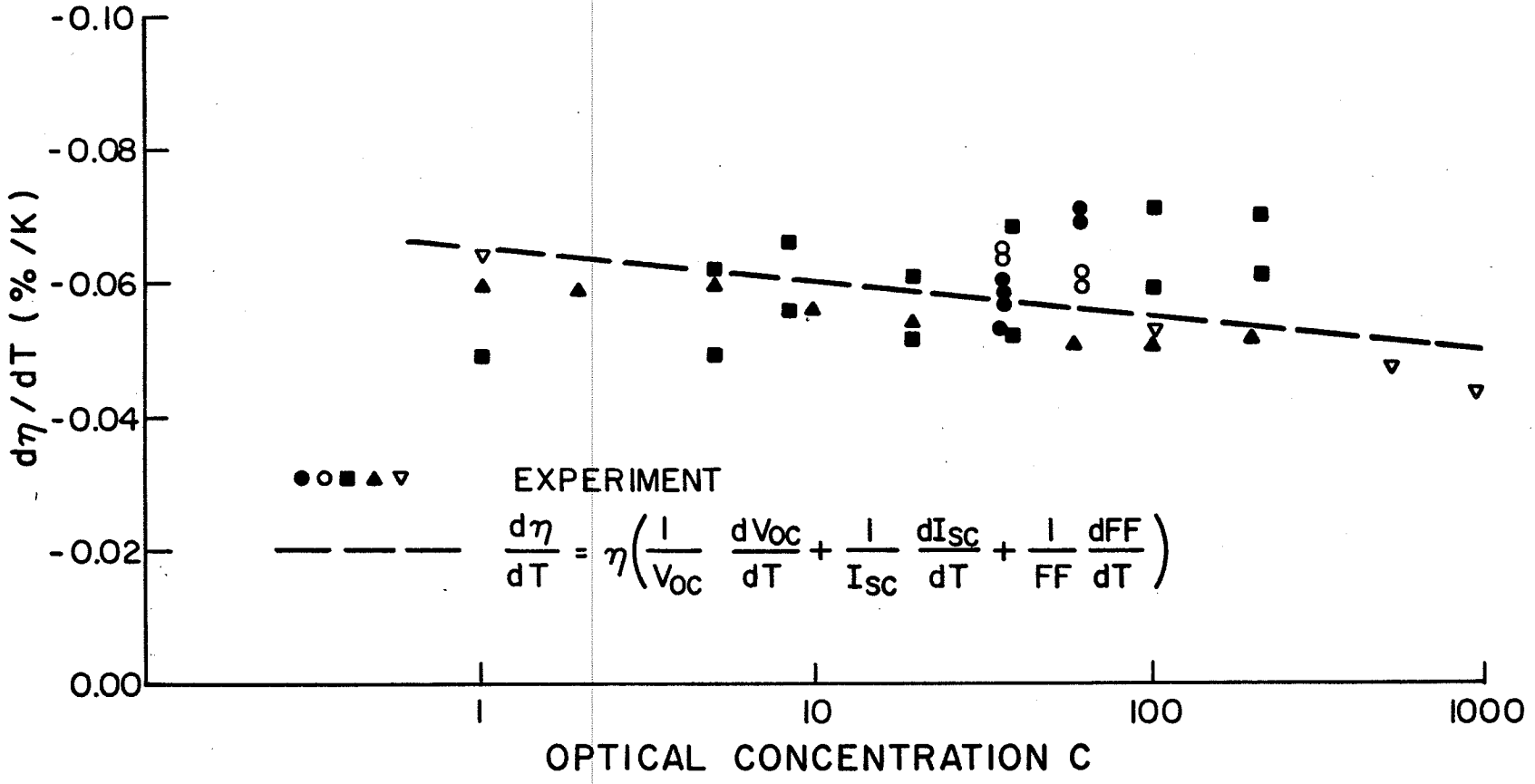
-0.10
-0.08
-0.06
-0.04
-0.02
0.00
dη / dT (% /K)
EXPERIMENT
$\frac{d\eta}{dT} = \eta\left(\frac{1}{V_{OC}}\frac{dV_{OC}}{dT} + \frac{1}{I_{SC}}\frac{dI_{SC}}{dT} + \frac{1}{FF}\frac{dFF}{dT}\right)$
1
10
100
1000
OPTICAL CONCENTRATION C

Fig. 11

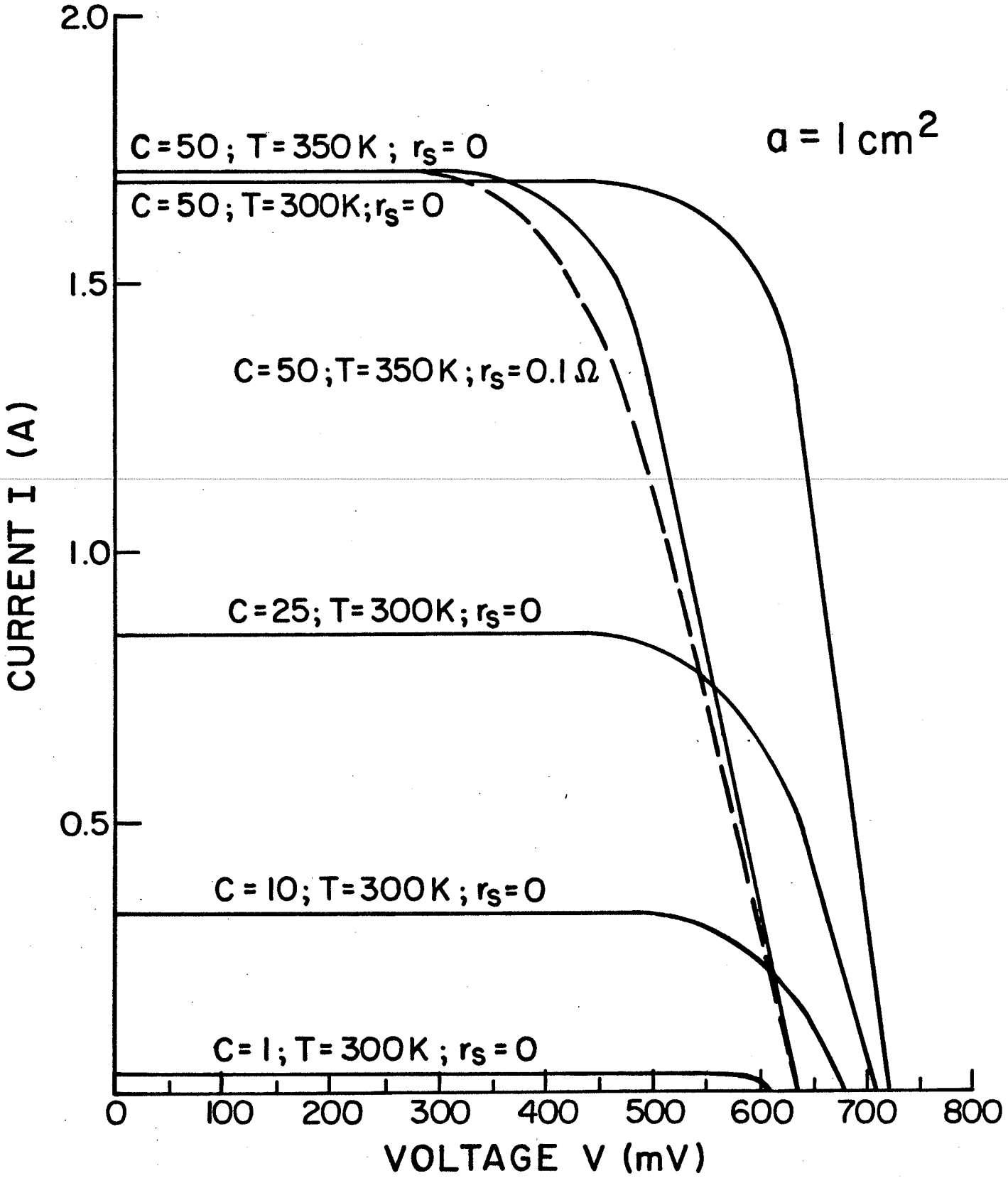
2.0
1.5
1.0
0.5
CURRENT I (A)
a = 1 cm²
C=50; T=350K; rs=0
C=50; T=300K; rs=0
C=50; T=350K; rs=0.1 Ω
C=25; T=300K; rs=0
C=10; T=300K; rs=0
C=1; T=300K; rs=0
0
100
200
300
400
500
600
700
800
VOLTAGE V (mV)

Fig. 12

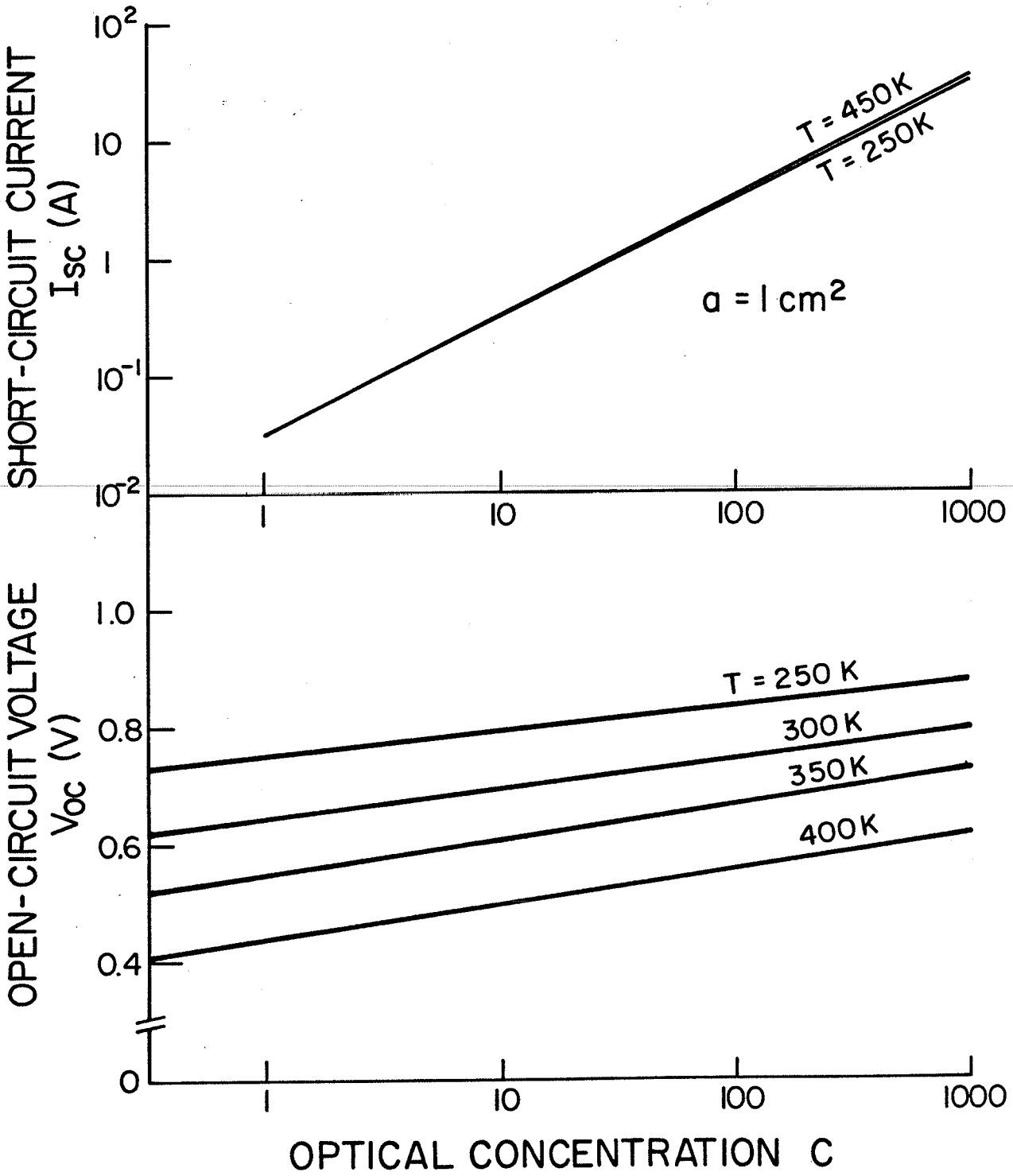
SHORT-CIRCUIT CURRENT
Isc (A)
10²
10
1
10⁻¹
10⁻²
T = 450K
T = 250K
a = 1 cm²
1
10
100
1000
OPEN-CIRCUIT VOLTAGE
Voc (V)
1.0
0.8
0.6
0.4
0
T = 250 K
300 K
350K
400K
1
10
100
1000
OPTICAL CONCENTRATION C

Fig. 13

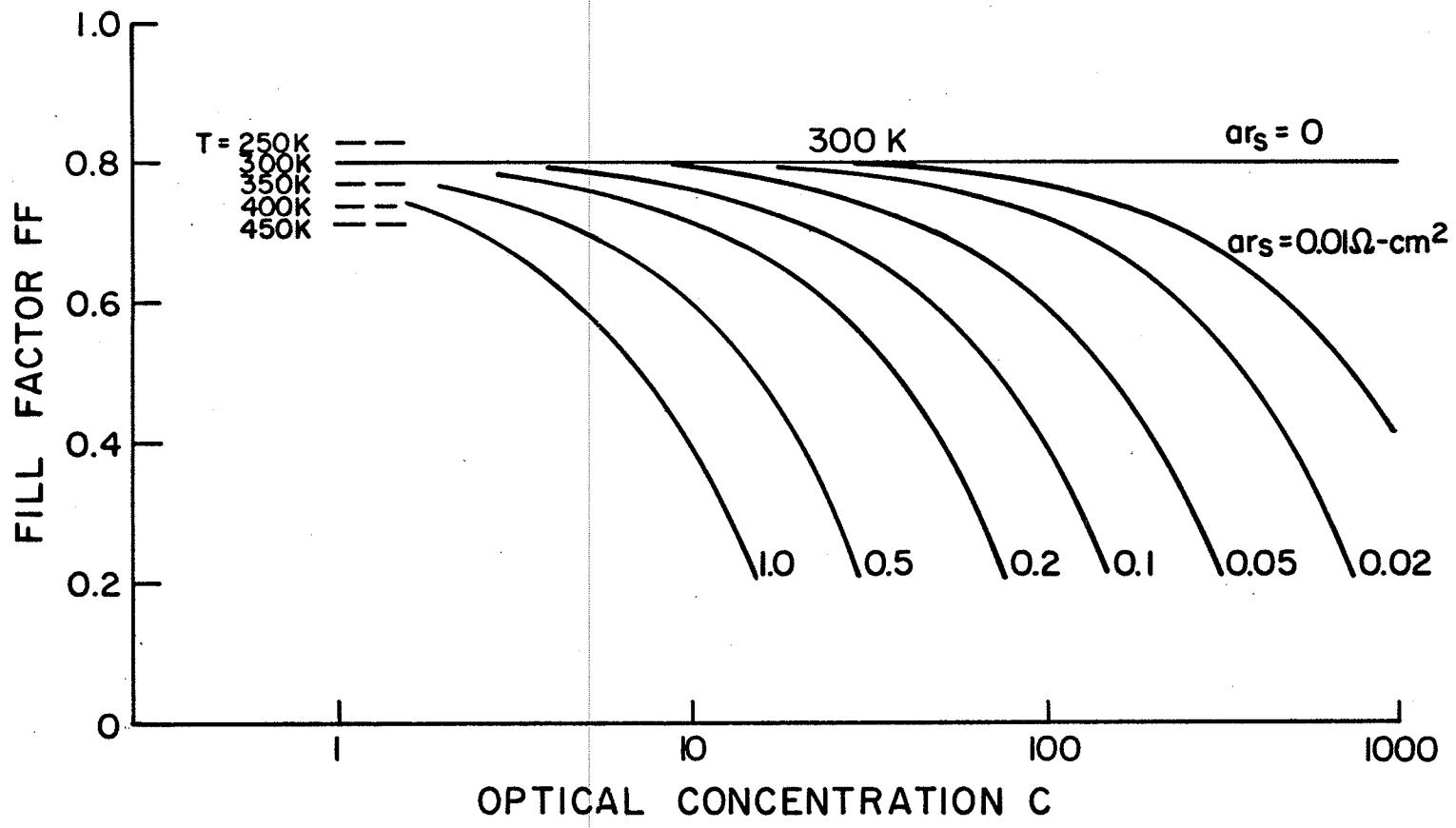
1.0
0.8
0.6
0.4
0.2
0
FILL FACTOR FF
T = 250K
300K
350K
400K
450K
300 K
$ar_s = 0$
$ar_s = 0.01\Omega\text{-cm}^2$
1.0
0.5
0.2
0.1
0.05
0.02
1
10
100
1000
OPTICAL CONCENTRATION C

Fig. 14

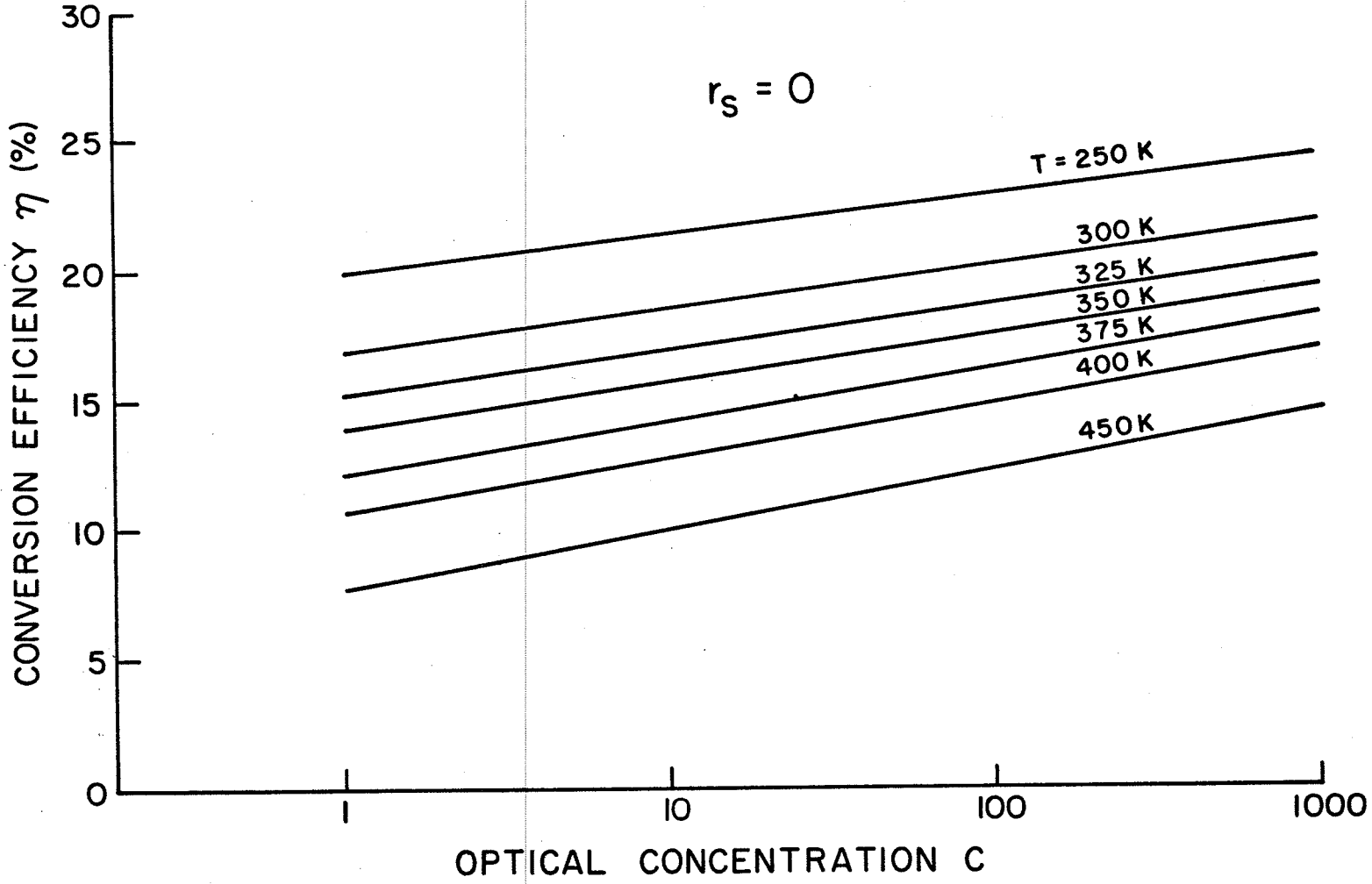
$r_s = 0$
T = 250 K
300 K
325 K
350 K
375 K
400 K
450K
CONVERSION EFFICIENCY $\eta$ (%)
30
25
20
15
10
5
0
1
10
100
1000
OPTICAL CONCENTRATION C

Fig. 15

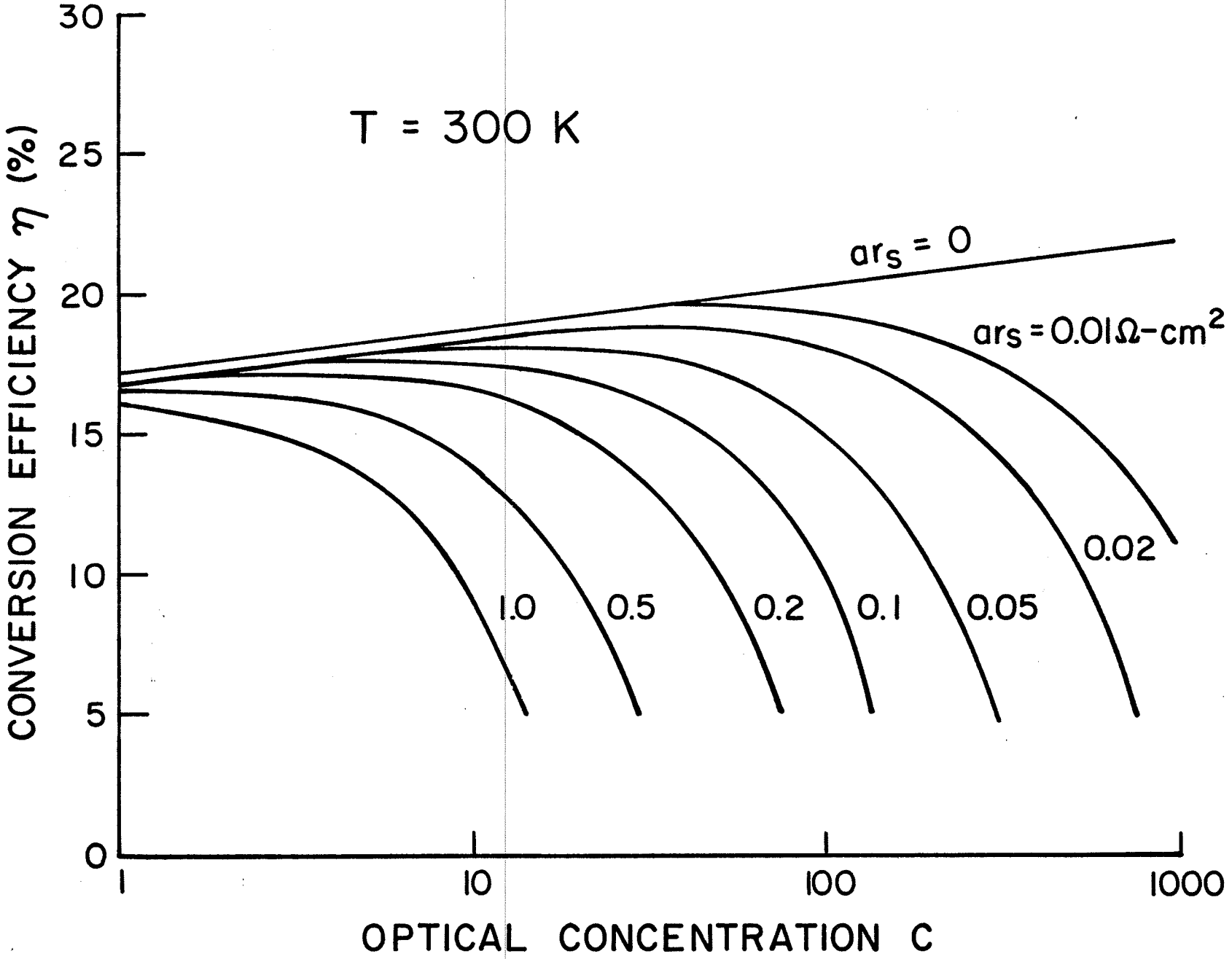
T = 300 K
CONVERSION EFFICIENCY η (%)
OPTICAL CONCENTRATION C
30
25
20
15
10
5
0
1
10
100
1000
$ar_s = 0$
$ar_s = 0.01\Omega\text{-cm}^2$
0.02
0.05
0.1
0.2
0.5
1.0

Fig. 16

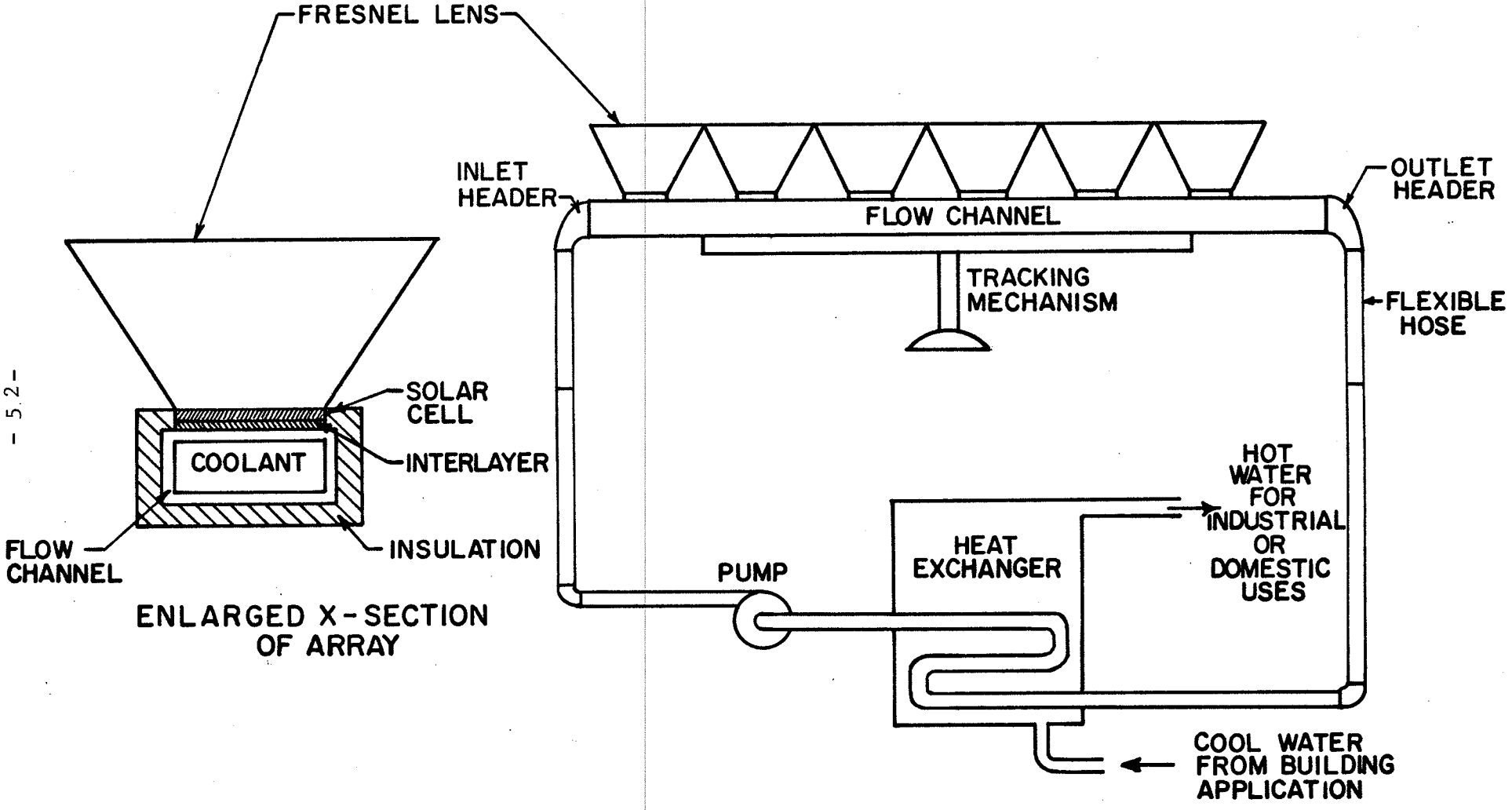
FRESNEL LENS
INLET HEADER
OUTLET HEADER
FLOW CHANNEL
TRACKING MECHANISM
FLEXIBLE HOSE
SOLAR CELL
INTERLAYER
COOLANT
FLOW CHANNEL
INSULATION
ENLARGED X-SECTION OF ARRAY
PUMP
HEAT EXCHANGER
HOT WATER FOR INDUSTRIAL OR DOMESTIC USES
COOL WATER FROM BUILDING APPLICATION

Fig. 17

# CHAPTER IV

## CONCLUSIONS

In this chapter we report the major conclusions of the investigations presented in Chapters 2 and 3. These conclusions relate (a) to experimental spectral response studies in cast silicon, and (b) to the modelling of silicon cells for solar concentrator systems.

(a) It is a property of recombination through extended defects (dislocations, grain boundaries) in extrinsic silicon that the recombination lifetime of minority carriers may be appreciably enhanced by relatively low levels of optical illumination (below AM1). This is not the case for extrinsic crystalline silicon in which recombination occurs through point defects. The origin of the difference is the space-charge regions which accompany extended defects, and which lead to the onset of high-injection conditions at the defect sites at low illumination levels. This also results in a simple modification of the expression for capture cross sections of these defects. The present model accounts for our experimental observations (1) that the quantum efficiency at long wavelengths, of solar cells on silicon containing extended defects, is substantially improved by an optical bias, (2) that the photocurrents in these devices are not appreciably reduced below those in Czochralski silicon cells, and (3) that the improvement of spectral response in the crystalline case can only occur at much higher optical intensities (concentrated sunlight), when high-level injection conditions are achieved in the bulk of the silicon.

(b) It has been possible to develop a very simple semiempirical model of silicon solar cells for concentrator applications, with explicit dependences upon optical concentration (C) and operating temperature (T). This model allows for the independent determination of all of the relevant photovoltaic parameters, and in particular of the photovoltaic conversion efficiency under arbitrary load conditions. Comparisons with experimental data on a variety of concentrator cells indicates that the predicted photovoltaic conversion efficiency is within 5% of the experimental value of most well-designed cells. In addition, photovoltaic parameters can be specified over the useful range of C and T to within approximately 10%. An illustration has been given of the design of a concentrator photovoltaic system with active cooling, in which the present model would be useful in the optimization of the temperature profile over the devices in the photovoltaic array.

References


1. E. Fabre, M. Mautref and A. Mircea, "Trap Saturation in Silicon Solar Cells", Appl. Phys. Lett., Vol. 27, pp. 239-241, Aug. 1975.

2. V. L. Dalal and A. R. Moore, "Design Considerations for High-Intensity Solar Cells", J. Appl. Phys., Vol. 48, pp. 1244-1251, March 1977.

3. C. T. Ho, R. O. Bell and F. V. Wald, "Enhancement of Diffusion Length in EFG Ribbon Solar Cells under Illumination", App. Phys. Lett., Vol. 31, pp. 463-465, October 1977.

4. A. Pogany, "Variation of Diffusion Length of Ribbon-Si Solar Cells with Light Intensity", Proc. 14th IEEE Phot. Spec. Conf., San Diego, CA, pp. 410-413, January 1980.

5. C. T. Ho and J. D. Mathias, "Effect of Short Wavelength Illumination of the Characteristic Bulk Diffusion Length in Ribbon Silicon Solar Cells", Solid St. Electron, Vol. 24, pp. 115-120, 1981.

6. R. D. Nasby, C. M. Garner, H. T. Weaver, F. W. Sexton and J. L. Rodriguez, "Characterization of p+nn+ Silicon Concentrator Solar Cells", Proc. 15th IEEE Phot. Spec. Conf., Kissimmee, Florida, pp. 132-137, 1981.

7. R. W. Sanderson and C. E. Backus, "The Behaviour of Silicon Concentrator Solar Cells Between 50 and 500 Suns", Proc. 15th IEEE Phot. Spec. Conf., Kissimmee, Florida, pp. 156-159, 1981.

8. V. Augelli, L. Vasanelli, M. Leo, R. A. Leo and G. Soliani, "Nonlinear Behaviour of the Short Circuit Current of a Solar Cell with Minority Carrier Lifetime Dependent on the Light Intensity", J. Appl. Phys., Vol. 53, pp. 1558-1562, March 1982.

9. V. Heine, "Dangling Bonds and Dislocations in Semiconductors", Phys. Rev., Vol. 146, pp. 568-570, June 1966.

10. H. C. Card and E. S. Yang, "Electronic Processes at Grain Boundaries in Polycrystalline Semiconductors under Optical Illumination", IEEE Trans. on Electron Dev., Vol. ED-24, pp. 397-402, April 1977.

11. C. H. Seager, "Electronic Properties of Semiconductor Grain Boundaries", pp. 85-98, in Grain Boundaries in Semiconductors, H. J. Leamy, G. E. Pike and C. H. Seager, editors, North Holland, New York, 1982.

12. W. Shockley and W. T. Read, Jr., "Statistics of the Recombination of Holes and Electrons", Phys. Rev., Vol. 87, pp. 835-842, September 1952.

13. R. N. Hall, "Electron-Hole Recombination in Germanium", Phys. Rev., Vol. 87, p. 387, 1952.

14. S. M. Sze, Physics of Semiconductor Devices, 2nd Ed. Chap. 14; Wiley, New York, 1981.

15. R. B. Godfrey and M. A. Green, "High-Efficiency Silicon minMIS Solar Cells-Design and Experimental Results", IEEE Trans. on Electron Dev., Vol. ED-27, pp. 737-744, 1980.

16. D. J. Thomson and H. C. Card, "Grating Solar Cells: An Experimental Comparison of Alternative Structures", to be published.

17. C. H. Seager and G. E. Pike, "Grain Boundary States and Varistor Behavior in Silicon Bicrystals", Appl. Phys. Lett., Vol. 35, pp. 709-711, November 1979.

18. G. C. McGonigal, D. J. Thomson and H. C. Card, "Electronic Transport at Grain Boundaries in Silicon: Part II Experiment", Phys. Rev. B., to be published.

19. P. Panayotatos and H. C. Card, "Recombination Velocity at Grain Boundaries in Polycrystalline Silicon under Optical Illumination", IEEE Elec. Dev. Lett., Vol. EDL-1, pp. 263-266, December 1980.

20. S. J. Fonash, Solar Cell Device Physics, Academic Press: New York, Chap. 4, pp. 166-168, 1981.

21. H. F. Matare, Defect Electronics in Semiconductors, Wiley-Interscience: New York, Chap. 8, pp. 156-167, and Chap. 11, pp. 287-306, 1971.

22. M. A. Green, Solar Cells, Prentice-Hall, Englewood Cliffs, N.J., 1982, Chapter 11.

23. H. J. Hovel, Solar Cells, Academic Press, New York, 1975, Chapter 8.

24. D. L. Pulfrey, Photovoltaic Power Generation, Van Nostrand Reinhold, New York, 1978, Chapter 4.

25. E. C. Boes, B. D. Shafer, and D. G. Schueler, Solar Cells, Vol. 6, pp. 3-15, 1982.

26. R. J. Schwartz, Solar Cells, Vol. 6, pp. 17-38, 1982.

27. S. Khemthong and P. A. Iles, Solar Cells, Vol. 6, pp. 59-77, 1982.

28. R. D. Nasby, C. M. Garner, F. W. Sexton, J. L. Rodriguez, B. H. Rose, and H. T. Weaver, Solar Cells, Vol. 6, pp. 49-58, 1982.

29. R. I. Frank, J. L. Goodrich, and R. Kaplow, Proc. 15th IEEE Phot. Spec. Conf., pp. 423-430, 1980.

30. R. D. Nasby, C. M. Garner, H. T. Weaver, F. W. Sexton, and J. L. Rodriguez, Proc. 16th IEEE Phot. Spec. Conf., pp. 132-137, 1981.

31. R. W. Sanderson and C. E. Backus, Proc. 16th IEEE Phot. Spec. Conf., pp. 156-159, 1981.

32. P. E. Gray, IEEE Trans. on Electron. Dev., Vol. ED-17, pp. 384-385, 1970.

33. Y. C. Kao and D. K. Schroder, IEEE Trans. on Electron. Dev., Vol. ED-17, pp. 384-385, 1970.

34. J. E. Parrott, IEEE Trans. on Electron Dev., Vol. ED-21, pp. 89-93, 1974.

35. S. R. Dhariwal, L. S. Kothari, and S. C. Jain, IEEE Trans. on Electron. Dev., Vol. ED-23, pp. 504-507, 1976.

36. S. Khemthong, P. A. Iles, and F. Ho, Proc. 16th IEEE Phot. Spec. Conf., pp. 126-131, 1981.

37. J. G. Fossum and F. A. Lindholm, IEEE Trans. on Electron. Dev., Vol. ED-24, pp. 325-329,1977.

38. M. A. Wolf and M. Wolf, Proc. 16th IEEE Phot. Spec. Conf., pp. 387-393, 1981.

39. V. K. Tewary, L. S. Kothari and S. C. Jain, Appl. Phys. Lett., Vol. 37, pp. 58-59, 1980.

40. V. L. Dalal and A. R. Moore, J. Appl. Phys., Vol. 48, pp. 1244-1251, 1977.

41. C. Y. Wu and J. F. Chen, J. Appl. Phys., Vol. 53, pp. 3852-3858, 1982.

42. R. N. Hall, Solid St. Electron., Vol. 24, pp. 595-616, 1981.

43. S. M. Sze, Physics of Semiconductor Devices, 2nd Ed., Wiley, New York, 1981, Chapters 2 and 14.

44. S. J. Fonash, Solar Cell Device Physics, Academic Press, New York, 1981.

45. M. A. Green, Solid St. Electron., Vol. 24, pp. 788-789, 1981.

46. J. P. Holman, Heat Transfer, 4th Ed., Chap. 6, McGraw-Hill, 1976.

47. A. J. Chapman, Heat Transfer, 3rd Ed., Chap. 8, MacMillan, New York, 1974.

48. F. Kreith, Principles of Heat Transfer, 3rd Edition, Chap. 8, Harper and Row, New York, 1973.

49. D. Gartner, et al., Int. J. Heat and Mass Transfer, Vol. 17, pp. 1003-1018, 1974.

50. W. M. Kays and M. E. Crawford, Convective Heat and Mass Transfer, 2nd Edition, Chap. 13, McGraw-Hill, New York, 1980.